Title

Alzheimer risk-increasing TREM2 variant causes aberrant cortical synapse density and promotes network hyperexcitability in mouse models.

Permalink

https://escholarship.org/uc/item/0r38b76h

Authors

Das, Melanie
Mao, Wenjie
Voskobiynyk, Yuliya
et al.

Peer reviewed

Alzheimer risk-increasing TREM2 variant causes aberrant cortical synapse density and promotes network hyperexcitability in mouse models

Melanie Das[a], **Wenjie Mao**[a,1], **Yuliya Voskobiynyk**[a], **Deanna Necula**[a,b], **Irene Lew**[a,2], **Cathrine Petersen**[a,b], **Allie Zahn**[a], **Gui-Qiu Yu**[a], **Xinxing Yu**[a,3], **Nicholas Smith**[a,4], **Faten A. Sayed**[a,5], **Li Gan**[c], **Jeanne T. Paz**[a,b,d], **Lennart Mucke**[a,b,d,*]

[a]Gladstone Institute of Neurological Disease, Gladstone Institutes, San Francisco, CA 94158, USA

[b]Neuroscience Graduate Program, University of California, San Francisco, San Francisco, CA 94158, USA

[c]Helen and Robert Appel Alzheimer's Disease Research Institute, Weill Cornell Medicine, New York City, NY 10065, USA

[*]Corresponding author. Address: 1650 Owens Street San Francisco, CA 94158, lennart.mucke@gladstone.ucsf.edu.
[1]Present address: The Janssen Pharmaceutical Companies of Johnson & Johnson, San Diego, CA
[2]Present address: Gilead Sciences, Foster City, CA
[3]Present address: Revolution Medicines, Redwood City, CA
[4]Present address: Alkahest, San Carlos, CA
[5]Present address: Lyft, San Francisco, CA

Abbreviations: **Aβ,** amyloid beta; **AD,** Alzheimer's disease; **ADP,** adenosine di-phosphate and phosphate; **AIC,** Akaike information criterion; **AMPA,** α-amino-3-hydroxy-5-methyl-4-isoxazolepropionic acid; **APP,** amyloid precursor protein; **ATP,** adenosine triphosphate; **AUC,** area under the curve; **CD39,** Ectonucleoside triphosphate diphosphohydrolase-1; **DAPI,** $4',6$-diamidino-2-phenylindole; **dLFPs,** differential local field potentials; **EEG,** electroencephalogram; **EMG,** electromyography; *Entpd1*, ectonucleoside triphosphate diphosphohydrolase; **FAD,** familial Alzheimer's disease; **hAPP,** human amyloid precursor protein; **IP,** intraperitoneal; **KA,** kainic acid; **LFP,** local field potential; **P2RY12,** purinergic receptor P2Y, G-protein coupled, 12; **PBS,** phosphate-buffered saline; **PBST,** phosphate-buffered saline with Tween®; **SWD,** spike and wave discharge; **ThioS,** thioflavin S; **TNF-α,** tumor necrosis factor-α; **TREM2,** triggering receptor expressed on myeloid cells 2; *TREM2*-**R47H**, R47H variant of triggering receptor expressed on myeloid cells 2; **WT,** wildtype.

Declaration of Interests
None.

[d]Department of Neurology and Weill Institute for Neurosciences, University of California, San Francisco, San Francisco, CA 94158, USA

Abstract

The R47H variant of triggering receptor expressed on myeloid cells 2 (TREM2) increases the risk of Alzheimer's disease (AD). To investigate potential mechanisms, we analyzed knockin mice expressing human *TREM2*-R47H from one mutant mouse *Trem2* allele. *TREM2*-R47H mice showed increased seizure activity in response to an acute excitotoxin challenge, compared to wildtype controls or knockin mice expressing the common variant of human *TREM2*. *TREM2*-R47H also increased spontaneous thalamocortical epileptiform activity in *App* knockin mice expressing amyloid precursor proteins bearing autosomal dominant AD mutations and a humanized amyloid-β sequence. In mice with or without such *App* modifications, *TREM2*-R47H increased the density of putative synapses in cortical regions without amyloid plaques. *TREM2*-R47H did not affect synaptic density in hippocampal regions with or without plaques. We conclude that TREM2-R47H increases AD-related network hyperexcitability and that it may do so, at least in part, by causing an imbalance in synaptic densities across brain regions.

Keywords

Introduction

Microglia, the innate immune cells of the brain, express multiple gene products that affect the risk of developing Alzheimer's disease (AD) (Bellenguez et al., 2022). A prominent example is the triggering receptor expressed on myeloid cells 2 (TREM2), which belongs to the immunoglobulin superfamily and, in the brain, is expressed primarily by microglia (Jay et al., 2017; Ulland and Colonna, 2018; Deczkowska et al., 2020). Genetic variants that impair TREM2 functions increase AD risk in heterozygous carriers (Guerreiro et al., 2013; Jonsson et al., 2013; Jay et al., 2017; Song et al., 2017; Ulrich et al., 2017; Ulland and Colonna, 2018). Homozygous mutations that inactivate TREM2 cause Nasu-Hakola disease, which combines early-onset dementia with epilepsy and other abnormalities (Paloneva et al., 2002; Bianchin et al., 2004; Kaneko et al., 2010; Nakamagoe et al., 2011; Jay et al., 2017).

Like humans with AD, mouse models with cerebral accumulation of human amyloid-β (Aβ) have increased microglial expression of TREM2 (Melchior et al., 2010; Matarin et al., 2015; Zhou et al., 2020; Das et al., 2021; Schoch et al., 2021; Xia et al., 2022). Increasing TREM2 levels reduced amyloid pathology in such models (Lee et al., 2018; Schlepckow et al., 2020), whereas reducing TREM2 levels diminished the number of plaque-associated microglia and increased plaque-associated axonal dystrophy (Wang et al., 2016; Yuan et al., 2016), with variable effects on overall plaque burden (Ulrich et al., 2014; Ulrich et al., 2017; Ulland and Colonna, 2018; Wood et al., 2022).

Thus, the increased microglial expression of TREM2 in AD brains is more likely to represent an adaptive than a maladaptive or pathogenic process. This conclusion is further supported by recent studies demonstrating that reduced expression of TREM2 exacerbates epileptic activity in mice injected with an excitotoxin (Das et al., 2021) or placed under urethane anesthesia (Stoiljkovic et al., 2022). These findings raise the possibility that microglia require normal levels of TREM2 to effectively suppress network hyperexcitability, a term we will use synonymously with hypersynchronous and epileptiform network activity. The potential clinical significance of network hyperexcitability in regard to dementing disorders and related TREM2 variants is highlighted by studies demonstrating a faster cognitive decline in sporadic AD patients who have nonconvulsive epileptiform activity (Vossel et al., 2016; Horváth et al., 2021) or who carry the R47H variant of TREM2 (Del-Aguila et al., 2018), and by the association of dementia with seizures in Nasu-Hakola disease (Kaneko et al., 2010; Nakamagoe et al., 2011).

Although AD is associated with an increased incidence of generalized tonic-clonic seizures, such seizures are more common in autosomal dominant familial AD (FAD) than in sporadic AD (Palop and Mucke, 2016; Zarea et al., 2016; Voglein et al., 2019). However, a substantial proportion of patients with sporadic AD have "subclinical" nonconvulsive epileptiform activity, which occurs most frequently during sleep (Vossel et al., 2016; Horváth et al., 2017; Lam et al., 2020). Similar nonconvulsive epileptiform activity is found in human amyloid precursor protein (hAPP) transgenic mice (Palop and Mucke, 2016) and in *App* knockin mice whose *App* alleles carry FAD mutations and have a humanized Aβ sequence (Johnson et al., 2020). In hAPP transgenic mice, suppressing epileptiform activity with the antiepileptic drug levetiracetam reversed cognitive and synaptic deficits (Sanchez et al., 2012; Nygaard et al., 2015; Das et al., 2021) as well as aberrant microglial gene expression (Das et al., 2021; Onos et al., 2022), suggesting that these abnormalities are driven, at least in part, by epileptiform activity.

The R47H variant of human TREM2 increases AD risk by 2–4-fold (Guerreiro et al., 2013; Jonsson et al., 2013; Jay et al., 2017; Song et al., 2017; Ulrich et al., 2017; Ulland and Colonna, 2018). Here we show that heterozygous *TREM2*$^{H/+}$ knockin mice, in which one mouse *Trem2* allele was modified to encode the R47H variant of human TREM2 (Sayed et al., 2021), have increased epileptiform activity when injected with the proconvulsant kainic acid or bred onto a homozygous *App*$^{NL-G-F/NL-G-F}$ knockin background (Saito et al., 2014), as compared to controls. *TREM2*$^{H/+}$ knockin mice also had an increased cortical density of pre- and postsynaptic markers, an alteration that may reflect microglial deficits in synaptic pruning (Filipello et al., 2018; Gratuze et al., 2020; Scott-Hewitt et al., 2020) and could promote network hyperexcitability (Chu et al., 2010; Faria et al., 2017; Han et al., 2023).

Materials and Methods

Mice

All mice were maintained on a C57BL/6J background. *TREM2*$^{H/+}$ and *TREM2*$^{R/+}$ knockin mice, in which one mouse *Trem2* allele was modified to encode the R47H variant or the common variant of human *TREM2*, respectively (Sayed et al., 2021), were generated by Drs. Faten Sayed and Li Gan. *App*$^{NL-G-F/NL-G-F}$ knockin mice (Saito et al., 2014), in which

both mouse *App* alleles have a humanized Aβ sequence and carry the Swedish (KM to NL), Arctic (E to G), and Iberian (I to F) mutations that cause autosomal dominant AD in humans (Mullan et al., 1992; Nilsberth et al., 2001; Guerreiro et al., 2010), were obtained from Drs. Takashi Saito and Takaomi Saido (RIKEN); for brevity, these mice are referred to here as App^{FAD} mice. Experimental and control groups were sex-balanced, matched for age and background strain, and generated by the following breeding schemes.

To generate $TREM2^{H/+}$ or $TREM2^{R/+}$ mice and $Trem2^{+/+}$ littermate controls, male $TREM2^{H/+}$ or $TREM2^{R/+}$ mice were bred with WT female C57BL/6J mice obtained from the Jackson Laboratory (Stock # 000664). To generate $TREM2^{H/+}$ or $Trem2^{+/+}$ mice on the $App^{NL-G-F/NL-G-F}$ background, female $Trem2^{H/+}$ mice were first bred with male $App^{NL-G-F/+}$ mice from a different litter. Among the resulting offspring, male or female $TREM2^{H/+}/App^{NL-G-F/+}$ mice were bred with $Trem2^{+/+}/App^{NL-G-F/+}$ mice of the opposite sex from a different litter to generate experimental and control groups.

Genotyping was performed by PCR amplification of DNA extracted from mouse tail biopsies. DNA was extracted by incubating tail samples in lysis buffer containing proteinase K at 55 °C overnight. Lysates were centrifuged, diluted 1:50 in water, and 2 μl of diluted lysate was used for PCR amplification. To identify $TREM2^{H/+}$ and $TREM2^{R/+}$ mice, we used primer sets that recognize human *TREM2* (forward: 5'-AGCTCTTCAGAGGAAACTGGGG-3'; reverse: 5'-TCGTGTCGGTAGTGTCTGCT-3'). To identify $App^{NL-G-F/NL-G-F}$ mice, we used primer sets that differentiate WT (forward:5′-ATCTCGGAAGTGAAGATG-3′; reverse: 5′-TGTAGATGAGAACTTAAC-3′) from mutant (forward: 5′-ATCTCGGAAGTGAATCTA-3′; reverse: 5′-CGTATAATGTATGCTATACGAAG-3′) *App* as described (Saito et al., 2014).

Unless indicated otherwise, mice were housed in sex-matched groups of up to five mice per cage. They were maintained on a 12-h light/dark cycle, PicoLab Rodent Diet 5053 (Lab Supply), and *ad libitum* access to drinking water. All animal procedures were approved by the Institutional Animal Care and Use Committee of the University of California, San Francisco.

Kainic acid injections

Kainic acid (Tocris Bioscience) was dissolved in saline at a concentration of 5 mg/ml, aliquoted, stored at −20 °C, and used within a month. On the day of injection, an aliquot was thawed and diluted with saline to 1 mg/ml. One hour of baseline EEG recording was obtained before the injection. While mice were connected to the EEG recording device, kainic acid (5 mg/kg body weight) was injected intraperitoneally every 30 min for a total of four injections and a total dose of 20 mg/kg body weight. After the injections, mice were continuously monitored by EEG and video recordings for another 21 hours, as described below.

Video-EEG recordings

For the implantation of recording electrodes, mice were anesthetized with isoflurane. For the experiments in Fig. 1 and fig. S1, four Teflon-coated silver wire electrodes (0.125 mm diameter) were soldered to a multichannel connector to make EEG plugs. After a skin

incision, small holes were drilled through the skull for the intracranial implantation of electrodes. Recording electrodes were placed under the skull and over each parietal cortex (2 mm posterior to Bregma and 2 mm from the midline). Reference electrodes were placed over each frontal cortex (1 mm anterior to Bregma and 1 mm lateral from the midline). Dental cement was used to insulate the wires and fasten the connector to the skull. Animals were allowed to recover for 2 weeks before EEG recording started. Simultaneous video and EEG recordings were done with a PowerLab data acquisition system (ADInstruments) on freely moving mice in a clear recording chamber for up to 24 h. EEG signals were acquired at a sampling rate of 1000 Hz.

For the experiments in Fig. 2 and fig. S2, devices were custom-made using a Mill-Max base (ED90267-ND, Mill-Max) to collect electrical activity from multiple brain regions simultaneously. Each device contained screws to record EEG activity from the left and right S1 cortex (0.5 mm posterior from Bregma, 3.5 mm lateral from midline), tungsten depth electrodes targeting layers 2–3 and layer 5 of the right S1 cortex (1.3 mm posterior from Bregma, 3.5 mm lateral from midline), the right hippocampus (1.3 mm posterior from Bregma, 1.5 mm lateral from midline), and the right sensory thalamus (1.3 mm posterior from Bregma, 1.5 mm lateral from midline), and an electromyogram (EMG) tungsten wire to record deep parasagittal cervical muscle activity (see diagrams in Fig. 2, A and B). A ground screw was placed over the cerebellum (1 mm posterior and 0.5 mm lateral from Lambda). After electrode implantations under isoflurane anesthesia, mice were housed individually and allowed to recover for at least one week before recording. Electrocorticograms and thalamic local field potentials (LFPs) were recorded using an RZ5 signal processor and Synapse software (Tucker Davis Technologies) and sampled at 1017 Hz. Mice were continuously monitored during recordings with a video camera, which was synchronized to the signal acquisition through the RZ5. Recording sessions lasted on average 3.2 ± 0.1 h (mean ± s.e.m.), and the length of recording periods did not significantly differ among genotypes ($P = 0.08$ by one-way ANOVA). In mice that survived until the end of the experiment, the location of depth electrodes was validated by histology.

Analysis of electrophysiological recordings

For the detection of epileptiform spikes and electroencephalographic seizures (Fig. 1 and fig. S1), EEG recordings were analyzed with LabChart Pro software (ADInstruments). EEG signals were filtered through a 5 Hz high-pass filter, 100 Hz low-pass filter, and 60 Hz notch filter. To quantify individual epileptiform spikes, a macro written in LabChart was used to automatically quantify events with an amplitude 7-fold the root mean square of baseline and an absolute value of the second derivative of the EEG signal 7000 mV/s^2. Excitotoxin-induced electroencephalographic seizures were identified when the power of the EEG signal in the 20–60 Hz frequency range was 5-fold baseline for at least 5 s. Power spectral density was calculated by fast-Fourier transformation of the EEG signal for 1-s bins. Termination of seizures was defined by the return of 20–60 Hz frequency power to baseline (Sato and Woolley, 2016), and the total duration of each seizure was quantified. Baseline measurements were assessed in mice during periods of rest from a 20-min recording before the first kainate injection. Seizure behavior was quantified according to a modified Racine score adapted from studies in mouse models of epilepsy (Van Erum et al., 2019; Terzic et

al., 2021): 0, no abnormal behaviors; 1, freezing; 2, myoclonic jerks, head nodding, tail stiffening; 3, forelimb clonus while sitting; 4, forelimb clonus with rearing and falling; 5, tonic-clonic convulsions with jumping, running and loss of righting reflex.

For the detection and analysis of spontaneous spike-and-wave discharges (SWDs) (Fig. 2 and fig. S2), we used the Spike2 software (version 8.19a, Cambridge Electronic Design, Cambridge, UK) and the Integrated Development Environment PyCharm (version 2020.3.2 JetBrains) as described (Paz et al., 2007; Paz et al., 2013). Briefly, this method detected events [1 x the mean + 2 x the standard deviation] of the EEG power in the 6–10 Hz frequency range that lasted 1 s and contained both spike and wave complexes. Supra-threshold episodes with gaps <200 ms between them were combined into a single event.

All detected events were inspected by an investigator blinded to genotype and treatment, and potential artifacts caused by movements or electrical noise were rejected.

Histopathology

Methods for the immunostaining and quantification of synapses were adapted from previously published protocols (Sauerbeck et al., 2020; Verstraelen et al., 2020). Coronal sections (30 μm thick) of paraformaldehyde-fixed hemibrains were prepared with a freezing microtome (Leica). For immunostaining of synaptic proteins, free-floating sections were rinsed in phosphate-buffered saline (PBS) containing 0.1% Tween 20 detergent (PBST), blocked in 3% hydrogen peroxidase for 15 min, rinsed in PBST, and incubated in antigen retrieval buffer (0.1 M citric acid and 0.1 M sodium citrate, pH 6.0) for 10 min at 100 °C. Sections were rinsed twice in PBS, incubated for 1 h in a blocking solution containing 20% normal goat serum in PBST, and incubated in primary antibodies against bassoon (1:500; Synaptic Systems) or homer 1 (1:250; Synaptic Systems) at room temperature for 24 h. Antibody-labeled sections were washed in PBST and incubated with anti-rabbit or anti-mouse secondary antibody conjugated to Alexa-Fluor 594 or 647 (1:500; Invitrogen), respectively, for 2 h in the dark at room temperature. Sections were then washed 3 times in PBST, mounted onto charged glass slides, dried in the dark overnight, and incubated in the dark for 10 min in a 1:1 mixture of PBS and ethanol containing 0.0015% filtered Thioflavin S (ThioS, Millipore Sigma). Slides were washed three times in PBST, counterstained with Hoechst 3342 (1:10,000; Thermo-Fisher Scientific), coverslipped with Mowiol 4-88 (Millipore Sigma) diluted 1:10 in Citifluor AF300 (Electron Microscopy Sciences), and dried overnight in the dark at room temperature.

Brain sections were visually matched to coronal planes in the Allen Mouse Common Coordinate Framework using anatomical landmarks such as outlines of the cingulum bundle, corpus callosum and hippocampal CA1 region. Electrode tracts in the S1 somatosensory cortex served as additional alignment guides. Sections located 1.94–2.06 mm posterior from Bregma were imaged: 1.5–1.7 mm from midline for parietal cortex and 1.0–1.4 mm from midline for hippocampus. For the quantitative analysis of synaptic density, images were acquired on a Zeiss LSM880 microscope with an AiryScan detector using a 10x objective and a 60x oil objective with a 10x zoom. For each brain section, a map was created by capturing a 10x image, using DAPI and ThioS staining as a guide. Regions in the hippocampal CA1 stratum radiatum or parietal cortex that were either >20 μm or <10 μm

from the outer edge of a 120–150 μm^2 plaque were chosen for imaging. The objective was switched to a 60x oil immersion lens and a z-scan image of the central 14 μm of each region was captured. For each brain section, 1–2 images were captured per brain region, and 3–4 sections were analyzed per mouse.

After image acquisition, files were imported into Imaris for synaptic density quantification. For each channel, puncta of synaptic protein immunoreactivity were detected with the spot detector function, using an x-y size of 0.2 μm, a z size of 0.6 μm, and automated background subtraction. A z guard was applied to each image to exclude any puncta that intersected the image border. The same filters were applied for all images and the accuracy of the spot detection tool in identifying puncta was confirmed for each image by an investigator blinded to genotype. To quantify synaptic density, the number of spots was normalized to the estimated volume of each image. The spatial (x, y, and z) coordinates of each spot were exported into R for further analysis. Nearest neighbor analysis was performed with the *spatstat* package in R (Baddeley et al., 2015) to determine the Euclidean distance between each bassoon-positive puncta and the nearest homer 1-positive puncta. Bassoon and homer 1 puncta separated by a distance of <0.5 μm were defined as putative synapses (Sauerbeck et al., 2020).

For the quantitative analysis of ThioS-labeled plaques, three hemibrain sections per mouse were imaged on a wide-field epifluorescence microscope (Keyence) using a 10x objection. Entire hemibrain sections were captured and plaques in the hippocampus were analyzed in FIJI (Schindelin et al., 2012). For each section, the region of interest (ROI) was defined as the outer border of the hippocampus, outlined with the pen tool, and converted into a binary (black and white) image. The Analyze Particles plugin was used to count the number of ThioS-positive plaques within each ROI. The number of plaques was normalized to the total area of each ROI. Plaques touching the border of the ROI were excluded from analysis. For each plaque within the ROI, the area occupied, circularity and average pixel intensity were recorded.

Statistical analyses

All statistical analyses were performed with R Statistical Software (version 4.2.0; R Foundation for Statistical Computing, Vienna, Austria). Statistical tests used, biological *n*, and definitions of significance are described in the figure legends.

Because some mice had no spikes or SWDs at some of the timepoints analyzed, these data did not meet the expectation that residuals are distributed normally, a key requirement for ANOVA tests. We therefore used alternative approaches to compare the occurrence of these electrophysiological events across groups and ages. For comparisons of spike counts following KA injections across groups, generalized linear models were used to assess differences between groups. For comparisons of SWD occurrence across multiple age groups, a generalized linear mixed-effects model was used to assess genotype differences. For both measures, the occurrence of electrophysiological events was modeled using discrete probability distributions (Poisson distribution and Negative Binomial distribution), which are appropriate for discrete, count-like data that are not normally distributed (Laird and Ware, 1982; Bates et al., 2015). Results from the model with the lower Akaike information

criterion (AIC) (Akaike, 1974) were reported. Pairwise comparisons were conducted for each model using estimated marginal means (Lenth et al., 2022), and *P* values were adjusted for multiple comparisons by the Holm-Sidak procedure.

For comparisons of continuous quantitative data, one- or two-way ANOVA was used, followed by post hoc Tukey tests for pairwise comparisons between groups. We used the Shapiro-Wilk test to assess whether the residuals were distributed normally. For data that did not pass normality assumptions, a Kruskal-Wallis test was used, followed by post hoc Mann-Whitney tests for pairwise comparisons between groups. For data that did pass normality assumptions, we used the Bartlett test for homogeneity of variances. For data that did not pass homogeneity of variance assumptions, Welch's one-way ANOVA was used, followed by post hoc Games-Howell tests for pairwise comparisons between groups.

Fisher's exact test was used to compare proportions of male and female mice with SWDs. To identify pairwise differences, a post-hoc Fisher's exact test was applied, followed by the Holm-Sidak procedure to adjust for multiple comparisons.

Tables S1 to S5 provide a summary of model specifications and results from all models used.

Results

Exacerbated epileptiform activity in kainic acid-challenged *Trem2*^H/+ knockin mice

Although AD increases the incidence of convulsive seizures, such seizures and their escalation into status epilepticus are relatively rare in this condition (Scarmeas et al., 2009; Palop and Mucke, 2016; Lam and Noebels, 2020). However, a substantial proportion of AD patients have non-convulsive epileptiform activity (Vossel et al., 2016; Horváth et al., 2017; Lam et al., 2017; Lam et al., 2020; Horváth et al., 2021). To assess the potential impact of R47H-variant human TREM2 on the latter type of particularly AD-relevant network dysfunction, we modified repeated low-dose kainic acid (KA) injection paradigms described by others (Hellier and Dudek, 2005; Tse et al., 2014; Umpierre et al., 2016) to elicit primarily non-convulsive epileptiform spike activity, relatively few convulsive seizures, and no status epilepticus.

TREM2^H/+ knockin mice (Sayed et al., 2021) received four intraperitoneal (IP) injections of saline (control) or KA (5 mg/kg), 30 min apart. Additional controls consisted of age- and sex-matched *TREM2*^R/+ knockin mice, in which one mouse *Trem2* allele was modified to encode the common variant (R47) of human TREM2 and which expressed similar levels of human TREM2 as *TREM2*^H/+ mice (Sayed et al., 2021), as well as *Trem2*^+/+ (WT) littermates from each *Trem2* knockin line. Since female sex seems to increase the biological effects of TREM2 hypofunction (Sayed et al., 2021; Essex et al., 2022), we focused these initial studies on female mice. Because one would expect AD-relevant pathomechanisms to be age-dependent, we assessed replicate groups of mice at two ages.

Since both seizures and individual epileptiform spikes can provide evidence for AD-relevant network hyperexcitability, we used intracranial electroencephalography (EEG) to quantify

cumulative cortical spike counts, including spikes that formed part of a seizure ("ictal spikes") and intermittent single spikes that occurred between or independent of seizures ("interictal spikes") (Fig. 1). At 5–6 months of age, $TREM2^{H/+}$ mice had an increased number of epileptiform spikes after the KA challenge, as compared to controls (Fig. 1, A to E). Biological n, statistical tests used, and definitions of significance are described in figure legends and Methods. For additional statistical details, see tables S1 to S5.

In all groups, the majority of spikes were interictal rather than ictal (Fig. 1, D and E), consistent with the mild KA challenge used, which elicited only a small number of seizures of relatively short durations (Fig. 1, F and G). None of the mice developed status epilepticus. Although the largest number of seizures and longest cumulative time spent in seizures were observed in $TREM2^{H/+}$ mice, these measures did not significantly differ among groups (Fig. 1, F and G). However, maximal KA-induced spike frequencies in $TREM2^{H/+}$ mice clearly exceeded those of all other groups (Fig. 1H). Notably, $TREM2^{R/+}$ mice expressing the common variant of human TREM2 did not differ from WT mice in any of the above measures (Fig. 1, B to H). At 2–3 months, the four groups of mice had comparable levels of KA-induced epileptiform spike activity (fig. S1), suggesting that the impact of $TREM2^{H/+}$ on KA-induced network hyperexcitability is age-dependent.

No differences in epileptiform spike activity were observed among genotypes during 20-min recordings that immediately preceded the KA injections or that followed them by 20 h (fig. S2). $TREM2^{R/+}$ mice were not included in the subsequent components of this study because their extent of KA-induced epileptiform activity did not differ from that of WT controls (Fig. 1, B to H and fig. S1, B to H).

$TREM2^H$ increases spontaneous epileptiform activity in untreated App^{FAD} mice

The findings described above indicate that $TREM2^H$ exacerbates epileptiform activity caused acutely by an excitotoxin. To determine whether $TREM2^H$ also exacerbates epileptiform activity caused by chronic expression of FAD-mutant APP/Aβ, we crossed $TREM2^{H/+}$ mice onto a homozygous $App^{NL-G-F/NL-G-F}$ background (Saito et al., 2014). From here on, we will refer to $App^{NL-G-F/NL-G-F}$ mice as App^{FAD} mice for brevity. Like hAPP transgenic mice, App^{FAD} mice develop prominent amyloid pathology and nonconvulsive epileptiform activity (Johnson et al., 2020). However, the relative preponderance of specific epileptiform events can differ among models. For example, compared to hAPP-J20 transgenic mice, App^{FAD} mice have fewer individual epileptiform spikes but more spike-and-wave discharges (SWDs) (Johnson et al., 2020).

To assess the effect of $TREM2^H$ on epileptiform activity in App^{FAD} mice, we recorded surface EEG activity from the S1 somatosensory cortex of female and male $Trem2^{+/+}$ (WT), $TREM2^{H/+}$, $Trem2^{+/+}/App^{FAD}$, and $TREM2^{H/+}/App^{FAD}$ mice at 10–12, 13–15, and 16–18 months of age. Depth electrodes were used to measure LFPs and multi-unit firing activity from the thalamus and hippocampus of the same mice. In contrast to $Trem2^{+/+}$ and $TREM2^{H/+}$ mice, $Trem2^{+/+}/App^{FAD}$ and $TREM2^{H/+}/App^{FAD}$ mice had spontaneous SWDs that were detected concomitantly in the EEG and in thalamic, but not hippocampal, field potentials (Fig. 2, A to C and fig. S3). These discharges were characterized by 8–9 Hz peak frequency in the spectrogram (Fig. 2, A to C), occurred during wakefulness, and were

associated with behavioral arrest (Fig. 2A). In combination with the absence of SWDs in WT controls, these characteristics make it likely that the SWDs of $Trem2^{+/+}/App^{FAD}$ and $TREM2^{H/+}/App^{FAD}$ mice represent abnormal epileptiform events. With aging, the frequency of these SWDs increased to higher levels in $TREM2^{H/+}/App^{FAD}$ than $Trem2^{+/+}/App^{FAD}$ mice (Fig. 2, D and E), indicating that $TREM2^{H}$ also exacerbates the epileptiform activity caused by FAD-mutant APP. The proportion of mice that exhibited at least one SWD during the recording was lower in female than male $Trem2^{+/+}/App^{FAD}$ mice but similar to male $Trem2^{+/+}/App^{FAD}$ mice in both male and female $TREM2^{H/+}/App^{FAD}$ mice (Fig. 2F).

Increased cortical density of synaptic markers in $TREM2^{H/+}/App^{+/+}$ and $TREM2^{H/+}/App^{FAD}$ mice

At 21–22 months of age, $TREM2^{H/+}/App^{FAD}$ mice did not differ from $Trem2^{+/+}/App^{FAD}$ mice in regard to the number, size, and fluorescence intensity of thioflavin S (ThioS)-positive amyloid plaques in the cortex and hippocampus (Fig. 3). These results are consistent with previous studies indicating that TREM2 hypofunction does not alter overall plaque burdens in mice producing human Aβ peptides (Ulrich et al., 2014; Yuan et al., 2016). See, however, refs. (Ulrich et al., 2017; Ulland and Colonna, 2018; Wood et al., 2022) for divergent results.

In addition to amyloid plaques, humans with AD and related mouse models have reduced densities of synapses in the cortex and hippocampus (Terry et al., 1991; Mucke et al., 2000; Chin et al., 2004; Morrison and Baxter, 2012). To assess the effect of $TREM2^{H}$ on synaptic densities, we colabeled brain sections from the different groups of mice with antibodies against the presynaptic protein bassoon and the postsynaptic protein homer 1. Pairs of bassoon-positive and homer 1-positive puncta that were <0.5 μm apart were defined as synaptic puncta (putative synapses) (Fig. 4A and ref. (Sauerbeck et al., 2020)).

We focused our synapse analysis on the parietal cortex because this brain region is affected by AD (deIpolyi et al., 2007; Jacobs et al., 2012) and shows extensive amyloid deposition as well as electrophysiological abnormalities in App^{FAD} mice (Saito et al., 2014; Whitesell et al., 2019; Johnson et al., 2020). In addition, its large size and uneven amyloid deposition facilitate the comparison of synaptic densities at different distances from plaques.

$TREM2^{H}$ increased the density of presynaptic, postsynaptic, and synaptic puncta in plaque-free areas of the parietal cortex in both $App^{+/+}$ and App^{FAD} mice, as compared to corresponding groups on the $Trem2^{+/+}$ background (Fig. 4, B to D). Adjacent to ThioS-positive plaques, $Trem2^{+/+}/App^{FAD}$ mice had reduced densities of presynaptic puncta and showed a trend toward reduced densities of postsynaptic and synaptic puncta, as compared to plaque-free areas of the parietal cortex (Fig. 4, E to G). Plaque-associated reductions of postsynaptic and synaptic puncta were greater and statistically more significant in $TREM2^{H/+}/App^{FAD}$ mice (Fig. 4, E to G), although this difference was caused, in good part, by the increased density of postsynaptic and synaptic puncta in plaque-free areas of their cortex (Fig. 4, E to G).

In contrast, $TREM2^{H}$ did not significantly change the density of presynaptic, postsynaptic, and synaptic puncta in plaque-free areas of the hippocampus in App^{FAD} or $App^{+/+}$ mice,

as compared to corresponding groups on the *Trem2*^{+/+} background (Fig. 5, A to C). The density of synaptic puncta was reduced in the vicinity of hippocampal plaques in both *Trem2*^{+/+}/*App*[FAD] and *TREM2*[H/+]/*App*[FAD] mice, and the latter group also had plaque-associated reductions in postsynaptic puncta (Fig. 5, D to F). In addition, trends toward plaque-associated reductions were observed for pre- and postsynaptic puncta in *Trem2*^{+/+}/ *App*[FAD] mice and for presynaptic puncta in *TREM2*[H/+]/*App*[FAD] mice (Fig. 5, D to F).

Discussion

Our findings suggest that the R47H variant of human TREM2 impairs the ability of microglia/macrophages to suppress network hyperexcitability caused either acutely by injection of an excitotoxin or chronically by expression of FAD-mutant APP/Aβ. These results are likely relevant to AD because this illness is associated with an increased risk of seizures (Palop and Mucke, 2016), nonconvulsive epileptiform activity (Vossel et al., 2016; Horváth et al., 2017; Lam et al., 2017; Lam et al., 2020), excitotoxicity-causing microinfarcts (Shih et al., 2013; Kalaria and Sepulveda-Falla, 2021), and the abnormal accumulation of APP metabolites (Multhaup et al., 2015; Haass and Selkoe, 2022). Since the detection of nonconvulsive epileptiform activity by EEG or magnetoencephalography predicts a faster cognitive decline in patients with sporadic AD (Vossel et al., 2016; Horváth et al., 2021), a reduced capacity of TREM2-R47H-expressing microglia to counteract this type of network dysfunction could contribute to the accelerated cognitive decline that has been observed in R47H carriers (Del-Aguila et al., 2018). Indeed, network hyperexcitability may promote the progression of AD by disrupting diverse aspects of the brain's "core homeostatic machinery" (Frere and Slutsky, 2018), including genome stability, proteostasis, energy metabolism, immune responses, and calcium homeostasis (Palop and Mucke, 2016; Frere and Slutsky, 2018; Shanbhag et al., 2019; Das et al., 2021; Ghatak et al., 2021).

Although R47H-variant TREM2 clearly increased the susceptibility to network hyperexcitability triggered by other pathogenic factors, it did not elicit epileptiform activity in the absence of such cofactors. In contrast, expression of FAD-mutant APP was sufficient to elicit such activity. These findings may be in line with the differential impact of these genetic alterations on AD development overall: autosomal dominant APP mutations typically cause early-onset AD with a high degree of penetrance, whereas R47H-variant TREM2 increases the relative risk of developing AD of later onset by 4-fold (Guerreiro et al., 2013; Jonsson et al., 2013; Karch and Goate, 2015; Jay et al., 2017; Song et al., 2017; Ulrich et al., 2017; Ulland and Colonna, 2018; Bellenguez et al., 2022).

Because heterozygous *Trem2* knockout (*Trem2*^{+/−}) mice also have a reduced seizure threshold after kainic acid injection (Das et al., 2021), it is likely that the increased seizure activity we detected in *TREM2*[H/+] mice after this challenge (relative to *TREM2*[R/+] and *Trem2*^{+/+} mice) and on the *App*[KI] background (relative to *Trem2*^{+/+} mice) reflects a hypofunction of R47H-variant human TREM2 relative to common variant human TREM2 or WT mouse TREM2. This conclusion is consistent with other lines of evidence supporting a hypofunction mechanism of TREM2 variants that increase the risk of AD or other dementias (Cheng-Hathaway et al., 2018; Sudom et al., 2018). It is interesting that the R47H substitution promotes the development of AD even when co-expressed

with an allele encoding unaltered and putatively fully functional mouse TREM2. Thus, to function properly, microglia/macrophages seem to require a specific level of TREM2 expression/activity, at least when responding to pathological challenges. Alternatively, disease-associated TREM2 variants may somehow counteract the functions of common variant TREM2. These possibilities are not mutually exclusive.

How exactly does TREM2 support, and TREM2 hypofunction impair, the ability of microglia to suppress network hyperexcitability? Although our study was not designed to conclusively answer this question, our quantification of synaptic puncta in different brain regions identified a potential mechanism that merits exploration in additional studies. Here, *TREM2*^{H} increased the density of putative synapses in the cortex, a brain region that showed exacerbated epileptiform activity in KA-treated *TREM2*$^{H/+}$ mice and untreated *TREM2*$^{H/+}$/*App*^{FAD} mice. In contrast, *TREM2*^{H} did not alter the density of putative synapses in the hippocampus, which did not show exacerbated epileptiform activity in *TREM2*$^{H/+}$/*App*^{FAD} mice. It is tempting to speculate that the excessive density of synapses in the cortex of *TREM2*$^{H/+}$ mice promotes the establishment of epileptogenic circuits after pathogenic cofactors such as excitotoxins or *App*^{FAD} trigger aberrant patterns of neuronal activity. Such a two-hit scenario is likely required for *TREM2*^{H} to promote epileptiform activity, as *TREM2*$^{H/+}$/*App*$^{+/+}$ and *TREM2*$^{H/+}$/*App*^{FAD} mice had comparable elevations in cortical synaptic puncta, only *TREM2*$^{H/+}$/*App*^{FAD} mice developed spontaneous epileptiform activity, and detecting an increased seizure risk in the *TREM2*$^{H/+}$/*App*$^{+/+}$ model required an excitotoxin challenge. The lack of spontaneous epileptiform activity in *TREM2*$^{H/+}$/*App*$^{+/+}$ mice further supports the notion that their increased cortical density of putative synapses is more likely a cause than a consequence of their reduced seizure threshold.

Notably, microglial "sculpting" of neural circuits by synaptic pruning occurs physiologically during brain development (Stevens et al., 2007; Schafer et al., 2012) and promotes the forgetting of remote memories in adult mice (Wang et al., 2020). It is conceivable that synaptic pruning by microglia also counteracts epileptogenesis, for example, by preventing the establishment of maladaptive circuits that promote network hyperexcitability (Chu et al., 2010; Faria et al., 2017; Han et al., 2023). In line with this hypothesis, complete ablation of *Trem2* reduced microglial activation after IP injection of KA (Zheng et al., 2017), and impaired synapse elimination, enhanced excitatory neurotransmission and reduced long-range functional connectivity during brain development (Filipello et al., 2018). Homozygous knockin rats expressing R47H-mutant rat TREM2 had enhanced AMPA receptor-mediated synaptic transmission and reduced long-term potentiation, and both abnormalities were reversed by treatment of hippocampal slices with a neutralizing antibody to TNF-α (Ren et al., 2020). Taken together, these findings suggest that TREM2 hypofunction variants may promote the development of epileptiform activity by impairing the ability of microglia to prune synaptic connections that become involved in the formation of maladaptive circuits after exposure to proepileptogenic conditions.

Several other signaling pathways have been implicated in the suppression of epileptic activity by microglia, but their potential links to TREM2 remain to be explored. Genetic ablation of the P2Y12 receptor, which mediates ATP-induced microglial process chemotaxis, reduced seizure-induced increases in microglial process numbers and

exacerbated kainate-induced seizure behaviors (Eyo et al., 2014). Microglia-specific deletion of *Entpd1*, which encodes the ATP/ADP-hydrolyzing ectoenzyme CD39, exacerbated pharmacologically-induced seizures (Badimon et al., 2020). Pharmacological blockade of microglial ATP/ADP sensing by inhibiting P2RY12 activity prevented the neuronal activity-induced recruitment of microglial processes (Badimon et al., 2020). Genetic inhibition of G_i-coupled signaling in microglia impaired microglial process motility, increased network hypersynchrony after physiologically evoked neuronal activity, and caused spontaneous seizures in mice (Merlini et al., 2021).

Our findings provide additional support for the notion that enhancing TREM2 activity could be of therapeutic benefit in AD and other dementias associated with hypofunction of TREM2 (Zheng et al., 2017; Lee et al., 2018; Lewcock et al., 2020; Schlepckow et al., 2020; Ferrara et al., 2022), and extend this concept to the suppression of network hyperexcitability. Indeed, additional studies are needed to explore whether TREM2 enhancement could counteract network hyperexcitability also in other conditions associated with excessive excitation/inhibition ratios, including epilepsies and neuropsychiatric disorders.

Limitations of the Study

The R47H variant of TREM2 increases AD risk in heterozygous human carriers (Guerreiro et al., 2013; Jonsson et al., 2013; Jay et al., 2017; Song et al., 2017; Ulrich et al., 2017; Ulland and Colonna, 2018). Because the other *TREM2* allele in these carriers encodes the common variant of human TREM2 rather than mouse TREM2, it would be interesting to repeat our analyses in *TREM2*[R/H] and *TREM2*[R/R] knockin mice expressing only human but not mouse TREM2. The potential sex effects shown in Fig. 2E and F may suggest that females can suppress *App*[FAD]-induced epileptiform activity more effectively than males but that their capacity to do so critically depends on TREM2, in line with other evidence indicating a greater susceptibility of females to TREM2 hypofunction (Sayed et al., 2021; Essex et al., 2022). However, because the number of mice we were able to analyze varied across experimental groups and was relatively small in some of them, larger cohorts of female and male mice should be tested to confirm the findings obtained in the current study. Because we obtained electrophysiological recordings from specific cortical, hippocampal, and thalamic subregions, we do not know if *TREM2*[H] also enhanced epileptiform activity in other brain regions that was not captured by our electrodes. It would also be interesting to explore whether the effects of *TREM2*[H] on AD-related epileptiform activity are influenced by brain states such as sleep and attentiveness. In the complex, multifactorial context of AD, TREM2 and microglia likely have direct and indirect interactions with additional pathogenic factors besides those investigated in the current study, including with tau and apolipoprotein E4 (Atagi et al., 2015; Yeh et al., 2016; Shi and Holtzman, 2018; Gratuze et al., 2020; Sayed et al., 2021). We used immunostaining for bassoon and homer 1 to estimate the density of putative synapses. However, additional approaches are required to confirm that changes in these markers are accompanied by changes in the corresponding synaptic structures. Particularly interesting questions to further pursue in this regard are whether the increased density of synaptic puncta we observed in the cortex of *TREM2*[H] mice represents an abnormal accumulation of synapses that are functional, cause aberrant excitation/inhibition ratios, promote the formation of epileptogenic circuits, and/or disrupt

network activity through other mechanisms. We did not resolve why *TREM2*[H] increased the density of synaptic puncta in the cortex but not the hippocampus, a finding that raises interesting questions about potential differences in the roles of TREM2 and microglia in the regulation of synapses across brain regions. Lastly, our study was not designed to causally link alterations in neural network activity to specific molecular or cellular alterations. Detailed comparisons of the ages at which these alterations first become detectable and follow-on perturbation analyses will be required to conclusively define such relationships.

Conclusions

The results of this study suggest that the AD risk-increasing R47H variant of TREM2 enhances neural hyperexcitability caused by excitotoxins or amyloid proteins, two factors implicated in the pathogenesis of AD. The imbalance in synaptic densities across brain regions we found in TREM2-R47H knockin mice could contribute to this effect through the formation of aberrant neuronal circuits. Since other studies have found nonconvulsive epileptiform activity to be associated with faster cognitive decline in patients with AD, a reduced capacity of TREM2-R47H-expressing microglia to counteract this type of network dysfunction could promote the development or progression of AD. Our findings support the notion that enhancing TREM2 activity could be of therapeutic benefit in AD and other dementias associated with hypofunction of TREM2, and incorporate into this concept the suppression of network hyperexcitability.

Supplementary Material

Refer to Web version on PubMed Central for supplementary material.

Acknowledgements

Data and Materials Availability

All data will be made available upon request.

References

Akaike H (1974). A new look at the statistical model identification. IEEE Trans. Autom. Control, 19, 716–723. doi:10.1109/TAC.1974.1100705.

Atagi Y, Liu CC, Painter MM, Chen XF, Verbeeck C, Zheng H, Li X, Rademakers R, Kang SS, Xu H, et al. (2015). Apolipoprotein E Is a ligand for triggering receptor expressed on myeloid cells 2 (TREM2). J. Biol. Chem, 290, 26043–26050. doi:10.1074/jbc.M115.679043. [PubMed: 26374899]

Baddeley A, Rubak E & Turner R 2015. Spatial point patterns: methodology and applications with R, New York, CRC press.

Badimon A, Strasburger HJ, Ayata P, Chen X, Nair A, Ikegami A, Hwang P, Chan AT, Graves SM, Uweru JO, et al. (2020). Negative feedback control of neuronal activity by microglia. Nature, 586, 417–423. doi:10.1038/s41586-020-2777-8. [PubMed: 32999463]

Bates D, Mächler M, Bolker B & Walker S (2015). Fitting linear mixed-effects models using lme4. J. Stat. Softw, 67, 1–48. doi:10.18637/jss.v067.i01.

Bellenguez C, Kucukali F, Jansen IE, Kleineidam L, Moreno-Grau S, Amin N, Naj AC, Campos-Martin R, Grenier-Boley B, Andrade V, et al. (2022). New insights into the genetic etiology of Alzheimer's disease and related dementias. Nat. Genet, 54, 412–436. doi:10.1038/s41588-022-01024-z. [PubMed: 35379992]

Bianchin MM, Capella HM, Chaves DL, Steindel M, Grisard EC, Ganev GG, Da Silva Junior JP, Neto Evaldo S, Poffo MA, Walz R, et al. (2004). Nasu-Hakola disease (polycystic lipomembranous osteodysplasia with sclerosing leukoencephalopathy--PLOSL): a dementia associated with bone cystic lesions. From clinical to genetic and molecular aspects. Cell. Mol. Neurobiol, 24, 1–24. doi:10.1023/b:cemn.0000012721.08168.ee. [PubMed: 15049507]

Cheng-Hathaway PJ, Reed-Geaghan EG, Jay TR, Casali BT, Bemiller SM, Puntambekar SS, Von Saucken VE, Williams RY, Karlo JC, Moutinho M, et al. (2018). The Trem2 R47H variant confers loss-of-function-like phenotypes in Alzheimer's disease. Mol. Neurodegener, 13, 1–12. doi:10.1186/s13024-018-0262-8. [PubMed: 29310663]

Chin J, Palop JJ, Yu G-Q, Kojima N, Masliah E & Mucke L (2004). Fyn kinase modulates synaptotoxicity, but not aberrant sprouting, in human amyloid precursor protein transgenic mice. J. Neurosci, 24, 4692–4697. [PubMed: 15140940]

Chu Y, Jin X, Parada I, Pesic A, Stevens B, Barres B & Prince DA (2010). Enhanced synaptic connectivity and epilepsy in C1q knockout mice. Proc. Natl. Acad. Sci. U. S. A, 107, 7975–7980. doi:10.1073/pnas.0913449107. [PubMed: 20375278]

Das M, Mao W, Shao E, Tamhankar S, Yu GQ, Yu X, Ho K, Wang X, Wang J & Mucke L (2021). Interdependence of neural network dysfunction and microglial alterations in Alzheimer's disease-related models. iScience, 24, 1. doi:10.1016/j.isci.2021.103245.

Deczkowska A, Weiner A & Amit I (2020). The physiology, pathology, and potential therapeutic applications of the TREM2 signaling pathway. Cell, 181, 1207–1217. doi:10.1016/j.cell.2020.05.003. [PubMed: 32531244]

deIpolyi AR, Rankin KP, Mucke L, Miller BL & Gorno-Tempini ML (2007). Spatial cognition and the human navigation network in AD and MCI. Neurology, 69, 986–997. [PubMed: 17785667]

Del-Aguila JL, Fernandez MV, Schindler S, Ibanez L, Deming Y, Ma S, Saef B, Black K, Budde J, Norton J, et al. (2018). Assessment of the genetic architecture of Alzheimer's disease risk in rate of memory decline. J. Alzheimers Dis, 62, 745–756. doi:10.3233/JAD-170834. [PubMed: 29480181]

Essex AL, Huot JR, Deosthale P, Wagner A, Figueras J, Davis A, Damrath J, Pin F, Wallace J, Bonetto A, et al. (2022). Triggering receptor expressed on myeloid cells 2 (TREM2) R47H variant causes distinct age- and sex-dependent musculoskeletal alterations in mice. J. Bone Miner. Res, 37, 1366–1381. doi:10.1002/jbmr.4572. [PubMed: 35575023]

Eyo UB, Peng J, Swiatkowski P, Mukherjee A, Bispo A & Wu LJ (2014). Neuronal hyperactivity recruits microglial processes via neuronal NMDA receptors and microglial P2Y12 receptors after status epilepticus. J. Neurosci, 34, 10528–10540. doi:10.1523/JNEUROSCI.0416-14.2014. [PubMed: 25100587]

Faria LC, Gu F, Parada I, Barres B, Luo ZD & Prince DA (2017). Epileptiform activity and behavioral arrests in mice overexpressing the calcium channel subunit alpha2delta-1. Neurobiol. Dis, 102, 70–80. doi:10.1016/j.nbd.2017.01.009. [PubMed: 28193459]

Ferrara SJ, Chaudhary P, Debell MJ, Marracci G, Miller H, Calkins E, Pocius E, Napier BA, Emery B, Bourdette D, et al. (2022). TREM2 is thyroid hormone regulated making the TREM2 pathway druggable with ligands for thyroid hormone receptor. Cell Chem. Biol, 29, 239–248 e4. doi:10.1016/j.chembiol.2021.07.014. [PubMed: 34375614]

Filipello F, Morini R, Corradini I, Zerbi V, Canzi A, Michalski B, Erreni M, Markicevic M, Starvaggi-Cucuzza C, Otero K, et al. (2018). The microglial innate immune receptor TREM2 is required for synapse elimination and normal brain connectivity. Immunity, 48, 979–991 e8. doi:10.1016/j.immuni.2018.04.016. [PubMed: 29752066]

Frere S & Slutsky I (2018). Alzheimer's disease: From firing instability to homeostasis network collapse. Neuron, 97, 32–58. doi:10.1016/j.neuron.2017.11.028. [PubMed: 29301104]

Ghatak S, Talantova M, Mckercher SR & Lipton SA (2021). Novel therapeutic approach for excitatory/inhibitory imbalance in neurodevelopmental and neurodegenerative diseases. Annu. Rev. Pharmacol. Toxicol, 61, 701–721. doi:10.1146/annurev-pharmtox-032320-015420. [PubMed: 32997602]

Gratuze M, Leyns CE, Sauerbeck AD, St-Pierre MK, Xiong M, Kim N, Serrano JR, Tremblay ME, Kummer TT, Colonna M, et al. (2020). Impact of TREM2R47H variant on tau pathology-induced gliosis and neurodegeneration. J. Clin. Invest, 130, 4954–4968. doi:10.1172/JCI138179. [PubMed: 32544086]

Guerreiro R, Wojtas A, Bras J, Carrasquillo M, Rogaeva E, Majounie E, Cruchaga C, Sassi C, Kauwe JS, Younkin S, et al. (2013). TREM2 variants in Alzheimer's disease. N. Engl. J. Med, 368, 117–127. doi:10.1056/NEJMoa1211851. [PubMed: 23150934]

Guerreiro RJ, Baquero M, Blesa R, Boada M, Bras JM, Bullido MJ, Calado A, Crook R, Ferreira C, Frank A, et al. (2010). Genetic screening of Alzheimer's disease genes in Iberian and African samples yields novel mutations in presenilins and APP. Neurobiol. Aging, 31, 725–731. doi:10.1016/j.neurobiolaging.2008.06.012. [PubMed: 18667258]

Haass C & Selkoe D (2022). If amyloid drives Alzheimer disease, why have anti-amyloid therapies not yet slowed cognitive decline? PLoS Biol, 20, e3001694. doi:10.1371/journal.pbio.3001694. [PubMed: 35862308]

Han RT, Vainchtein ID, Schlachetzki JCM, Cho FS, Dorman LC, Ahn E, Kim DK, Barron JJ, Nakao-Inoue H, Molofsky AB, et al. (2023). Microglial pattern recognition via IL-33 promotes synaptic refinement in developing corticothalamic circuits in mice. J. Exp. Med, 220, 1–19. doi:10.1084/jem.20220605.

Hellier JL & Dudek FE (2005). Chemoconvulsant model of chronic spontaneous seizures. Curr. Protoc. Neurosci, Chapter 9, 9.19.1–9.19.12. doi:10.1002/0471142301.ns0919s31.

Horváth A, Szucs A, Barcs G & Kamondi A (2017). Sleep EEG detects epileptiform activity in Alzheimer's disease with high sensitivity. J. Alzheimers Dis, 56, 1175–1183. doi:10.3233/JAD-160994. [PubMed: 28128769]

Horváth AA, Papp A, Zsuffa J, Szucs A, Luckl J, Radai F, Nagy F, Hidasi Z, Csukly G, Barcs G, et al. (2021). Subclinical epileptiform activity accelerates the progression of Alzheimer's disease: A long-term EEG study. Clin. Neurophysiol, 132, 1982–1989. doi:10.1016/j.clinph.2021.03.050. [PubMed: 34034963]

Jacobs HI, Van Boxtel MP, Jolles J, Verhey FR & Uylings HB (2012). Parietal cortex matters in Alzheimer's disease: an overview of structural, functional and metabolic findings. Neurosci. Biobehav. Rev, 36, 297–309. doi:10.1016/j.neubiorev.2011.06.009. [PubMed: 21741401]

Jay TR, Von Saucken VE & Landreth GE (2017). TREM2 in neurodegenerative diseases. Mol. Neurodegener, 12, 1–33. doi:10.1186/s13024-017-0197-5. [PubMed: 28049533]

Johnson ECB, Ho K, Yu GQ, Das M, Sanchez PE, Biljana D, Lopez I, Yu X, Gill M, Zhang W, et al. (2020). Behavioral and neural network abnormalities in human APP transgenic mice resemble those of App knock-in mice and are modulated by familial Alzheimer's disease mutations but not by inhibition of BACE1. Mol. Neurodegener, 15, 1–26. doi:10.1186/s13024-020-00393-5. [PubMed: 31964406]

Jonsson T, Stefansson H, Steinberg S, Jonsdottir I, Jonsson PV, Snaedal J, Bjornsson S, Huttenlocher J, Levey AI, Lah JJ, et al. (2013). Variant of TREM2 associated with the risk of Alzheimer's disease. N. Engl. J. Med, 368, 107–116. doi:10.1056/NEJMoa1211103. [PubMed: 23150908]

Kalaria RN & Sepulveda-Falla D (2021). Cerebral small vessel disease in sporadic and familial Alzheimer disease. Am. J. Pathol, 191, 1888–1905. doi:10.1016/j.ajpath.2021.07.004. [PubMed: 34331941]

Kaneko M, Sano K, Nakayama J & Amano N (2010). Nasu-Hakola disease: The first case reported by Nasu and review: The 50th Anniversary of Japanese Society of Neuropathology. Neuropathology, 30, 463–470. doi:10.1111/j.1440-1789.2010.01127.x. [PubMed: 20500450]

Karch CM & Goate AM (2015). Alzheimer's disease risk genes and mechanisms of disease pathogenesis. Biol. Psychiatry, 77, 43–51. doi:10.1016/j.biopsych.2014.05.006. [PubMed: 24951455]

Laird NM & Ware JH (1982). Random-effects models for longitudinal data. Biometrics, 38, 963–974. [PubMed: 7168798]

Lam AD, Deck G, Goldman A, Eskandar EN, Noebels J & Cole AJ (2017). Silent hippocampal seizures and spikes identified by foramen ovale electrodes in Alzheimer's disease. Nat. Med, 23, 678–680. doi:10.1038/nm.4330. [PubMed: 28459436]

Lam AD & Noebels J (2020). Night watch on the Titanic: detecting early signs of epileptogenesis in Alzheimer disease. Epilepsy Curr, 20, 369–374. doi:10.1177/1535759720964775. [PubMed: 33081517]

Lam AD, Sarkis RA, Pellerin KR, Jing J, Dworetzky BA, Hoch DB, Jacobs CS, Lee JW, Weisholtz DS, Zepeda R, et al. (2020). Association of epileptiform abnormalities and seizures in Alzheimer disease. Neurology, 95, e2259–e2270. doi:10.1212/WNL.0000000000010612. [PubMed: 32764101]

Lee CYD, Daggett A, Gu X, Jiang LL, Langfelder P, Li X, Wang N, Zhao Y, Park CS, Cooper Y, et al. (2018). Elevated TREM2 gene dosage reprograms microglia responsivity and ameliorates pathological phenotypes in Alzheimer's disease models. Neuron, 97, 1032–1048.e5. doi:10.1016/j.neuron.2018.02.002. [PubMed: 29518357]

Lenth RV, Bolker B, Buerkner P, Gine-Vazquez I, Herve M, Jung M, Love J, Miguez F, Riebl H & Singmann H 2022. emmeans: Estimated Marginal Means, aka Least-Squares Means. 1.8.7 ed.

Lewcock JW, Schlepckow K, Di Paolo G, Tahirovic S, Monroe KM & Haass C (2020). Emerging microglia biology defines novel therapeutic approaches for Alzheimer's disease. Neuron, 108, 801–821. doi:10.1016/j.neuron.2020.09.029. [PubMed: 33096024]

Matarin M, Salih DA, Yasvoina M, Cummings DM, Guelfi S, Liu W, Nahaboo Solim MA, Moens TG, Paublete RM, Ali SS, et al. (2015). A genome–wide gene-expression analysis and database in transgenic mice during development of amyloid or tau pathology. Cell Rep., 10, 633–644. doi:10.1016/j.celrep.2014.12.041. [PubMed: 25620700]

Melchior B, Garcia AE, Hsiung BK, Lo KM, Doose JM, Thrash JC, Stalder AK, Staufenbiel M, Neumann H & Carson MJ (2010). Dual induction of TREM2 and tolerance-related transcript, Tmem176b, in amyloid transgenic mice: implications for vaccine-based therapies for Alzheimer's disease. ASN Neuro., 2, 157–170. doi:10.1042/AN20100010.

Merlini M, Rafalski VA, Ma K, Kim KY, Bushong EA, Rios Coronado PE, Yan Z, Mendiola AS, Sozmen EG, Ryu JK, et al. (2021). Microglial Gi-dependent dynamics regulate brain network hyperexcitability. Nat. Neurosci, 24, 19–23. doi:10.1038/s41593-020-00756-7. [PubMed: 33318667]

Morrison JH & Baxter MG (2012). The ageing cortical synapse: Hallmarks and implications for cognitive decline. Nat. Rev. Neurosci, 13, 240–250. doi:10.1038/nrn3200. [PubMed: 22395804]

Mucke L, Masliah E, Yu G-Q, Mallory M, Rockenstein E, Tatsuno G, Hu K, Kholodenko D, Johnson-Wood K & Mcconlogue L (2000). High-level neuronal expression of Aβ_{1-42} in wild-type human amyloid protein precursor transgenic mice: Synaptotoxicity without plaque formation. J. Neurosci, 20, 4050–4058. doi:10.1523/JNEUROSCI.20-11-04050.2000. [PubMed: 10818140]

Mullan M, Crawford F, Axelman K, Houlden H, Lilius L, Winblad B & Lannfelt L (1992). A pathogenic mutation for probable Alzheimer's disease in the APP gene at the N-terminus of β-amyloid. Nat. Genet, 1, 345–347. doi:10.1038/ng0892-345. [PubMed: 1302033]

Multhaup G, Huber O, Buee L & Galas MC (2015). Amyloid Precursor Protein (APP) metabolites APP Intracellular Fragment (AICD), Abeta42, and Tau in nuclear roles. J. Biol. Chem, 290, 23515–23522. doi:10.1074/jbc.R115.677211. [PubMed: 26296890]

Nakamagoe K, Shioya A, Yamaguchi T, Takahashi H, Koide R, Monzen T, Satoh J & Tamaoka A (2011). A Japanese case with Nasu-Hakola disease of DAP12 gene mutation exhibiting precuneus hypoperfusion. Intern. Med, 50, 2839–2844. doi:10.2169/internalmedicine.50.5891. [PubMed: 22082900]

Nilsberth C, Westlind-Danielsson A, Eckman CB, Condron MM, Axelman K, Forsell C, Stenh C, Luthman J, Teplow DB, Younkin SG, et al. (2001). The 'Arctic' APP mutation (E693G) causes Alzheimer's disease by enhanced Aβ protofibril formation. Nat. Neurosci, 4, 887–893. [PubMed: 11528419]

Nygaard HB, Kaufman AC, Sekine-Konno T, Huh LL, Going H, Feldman SJ, Kostylev MA & Strittmatter SM (2015). Brivaracetam, but not ethosuximide, reverses memory impairments in an Alzheimer's disease mouse model. Alzheimer Res. Ther, 7, 1–12. doi:10.1186/s13195-015-0110-9.

Onos KD, Quinney SK, Jones DR, Masters AR, Pandey R, Keezer KJ, Biesdorf C, Metzger IF, Meyers JA, Peters J, et al. (2022). Pharmacokinetic, pharmacodynamic, and transcriptomic analysis of chronic levetiracetam treatment in 5XFAD mice: A MODEL-AD preclinical testing core study. Alzheimers Dement. (N. Y.), 8, 1–14. doi:10.1002/trc2.12329.

Paloneva J, Manninen T, Christman G, Hovanes K, Mandelin J, Adolfsson R, Bianchin M, Bird T, Miranda R, Salmaggi A, et al. (2002). Mutations in two genes encoding different subunits of a receptor signaling complex result in an identical disease phenotype. Am. J. Hum. Genet, 71, 656–662. doi:10.1086/342259. [PubMed: 12080485]

Palop JJ & Mucke L (2016). Network abnormalities and interneuron dysfunction in Alzheimer disease. Nat. Rev. Neurosci, 17, 777–792. doi:10.1038/nrn.2016.141. [PubMed: 27829687]

Paz JT, Chavez M, Saillet S, Deniau JM & Charpier S (2007). Activity of ventral medial thalamic neurons during absence seizures and modulation of cortical paroxysms by the nigrothalamic pathway. J. Neurosci, 27, 929–941. doi:10.1523/JNEUROSCI.4677-06.2007. [PubMed: 17251435]

Paz JT, Davidson TJ, Frechette ES, Delord B, Parada I, Peng K, Deisseroth K & Huguenard JR (2013). Closed-loop optogenetic control of thalamus as a tool for interrupting seizures after cortical injury. Nat. Neurosci, 16, 64–70. doi:10.1038/nn.3269. [PubMed: 23143518]

Ren S, Yao W, Tambini MD, Yin T, Norris KA & D'adamio L (2020). Microglia TREM2(R47H) Alzheimer-linked variant enhances excitatory transmission and reduces LTP via increased TNF-alpha levels. Elife, 9, 1–18. doi:10.7554/eLife.57513.

Saito T, Matsuba Y, Mihira N, Takano J, Nilsson P, Itohara S, Iwata N & Saido TC (2014). Single App knock-in mouse models of Alzheimer's disease. Nat. Neurosci, 17, 661–663. doi:10.1038/nn.3697. [PubMed: 24728269]

Sanchez PE, Zhu L, Verret L, Vossel KA, Orr AG, Cirrito JR, Devidze N, Ho K, Yu G-Q, Palop JJ, et al. (2012). Levetiracetam suppresses neuronal network dysfunction and reverses synaptic and cognitive deficits in an Alzheimer's disease model. Proc. Natl. Acad. Sci. USA, 109, E2895–E2903. doi:10.1073/pnas.1121081109. [PubMed: 22869752]

Sato SM & Woolley CS (2016). Acute inhibition of neurosteroid estrogen synthesis suppresses status epilepticus in an animal model. Elife, 5, 1–25. doi:10.7554/eLife.12917.

Sauerbeck AD, Gangolli M, Reitz SJ, Salyards MH, Kim SH, Hemingway C, Gratuze M, Makkapati T, Kerschensteiner M, Holtzman DM, et al. (2020). SEQUIN multiscale imaging of mammalian central synapses reveals loss of synaptic connectivity resulting from diffuse traumatic brain injury. Neuron, 107, 257–273 e5. doi:10.1016/j.neuron.2020.04.012. [PubMed: 32392471]

Sayed FA, Kodama L, Fan L, Carling GK, Udeochu JC, Le D, Li Q, Zhou L, Wong MY, Horowitz R, et al. (2021). AD-linked R47H-TREM2 mutation induces disease-enhancing microglial states via AKT hyperactivation. Sci. Transl. Med, 13, eabe3947. doi:10.1126/scitranslmed.abe3947. [PubMed: 34851693]

Scarmeas N, Honig LS, Choi H, Cantero J, Brandt J, Blacker D, Albert M, Amatniek JC, Marder K, Bell K, et al. (2009). Seizures in Alzheimer disease: Who, when, and how common? Arch. Neurol, 66, 992–997. doi:10.1001/archneurol.2009.130. [PubMed: 19667221]

Schafer DP, Lehrman EK, Kautzman AG, Koyama R, Mardinly AR, Yamasaki R, Ransohoff RM, Greenberg ME, Barres BA & Stevens B (2012). Microglia sculpt postnatal neural circuits in an activity and complement-dependent manner. Neuron, 74, 691–705. doi:10.1016/j.neuron.2012.03.026. [PubMed: 22632727]

Schindelin J, Arganda-Carreras I, Frise E, Kaynig V, Longair M, Pietzsch T, Preibisch S, Rueden C, Saalfeld S, Schmid B, et al. (2012). Fiji: an open-source platform for biological-image analysis. Nat. Methods, 9, 676–682. doi:10.1038/nmeth.2019. [PubMed: 22743772]

Schlepckow K, Monroe KM, Kleinberger G, Cantuti-Castelvetri L, Parhizkar S, Xia D, Willem M, Werner G, Pettkus N, Brunner B, et al. (2020). Enhancing protective microglial activities with a dual function TREM2 antibody to the stalk region. EMBO Mol. Med, 12, e11227. doi:10.15252/emmm.201911227. [PubMed: 32154671]

Schoch KM, Ezerskiy LA, Morhaus MM, Bannon RN, Sauerbeck AD, Shabsovich M, Jafar-Nejad P, Rigo F & Miller TM (2021). Acute Trem2 reduction triggers increased microglial phagocytosis, slowing amyloid deposition in mice. Proc. Natl. Acad. Sci. U S A, 118, 1–10. doi:10.1073/pnas.2100356118.

Scott-Hewitt N, Perrucci F, Morini R, Erreni M, Mahoney M, Witkowska A, Carey A, Faggiani E, Schuetz LT, Mason S, et al. (2020). Local externalization of phosphatidylserine mediates developmental synaptic pruning by microglia. EMBO J, 39, 1–20. doi:10.15252/embj.2020105380.

Shanbhag NM, Evans MD, Mao W, Nana AL, Seeley WW, Adame A, Rissman RA, Masliah E & Mucke L (2019). Early neuronal accumulation of DNA double strand breaks in Alzheimer's disease. Acta Neuropathol. Commun, 7, 1–18. doi:10.1186/s40478-019-0723-5.

Shi Y & Holtzman DM (2018). Interplay between innate immunity and Alzheimer disease: APOE and TREM2 in the spotlight. Nat. Rev. Immunol, 18, 759–772. doi:10.1038/s41577-018-0051-1. [PubMed: 30140051]

Shih AY, Blinder P, Tsai PS, Friedman B, Stanley G, Lyden PD & Kleinfeld D (2013). The smallest stroke: occlusion of one penetrating vessel leads to infarction and a cognitive deficit. Nat. Neurosci, 16, 55–63. doi:10.1038/nn.3278. [PubMed: 23242312]

Song W, Hooli B, Mullin K, Jin SC, Cella M, Ulland TK, Wang Y, Tanzi RE & Colonna M (2017). Alzheimer's disease-associated TREM2 variants exhibit either decreased or increased ligand-dependent activation. Alzheimers Dement, 13, 381–387. doi:10.1016/j.jalz.2016.07.004. [PubMed: 27520774]

Stevens B, Allen NJ, Vazquez LE, Howell GR, Christopherson KS, Nouri N, Micheva KD, Mehalow AK, Huberman AD, Stafford B, et al. (2007). The classical complement cascade mediates CNS synapse elimination. Cell, 131, 1164–1178. doi:10.1016/j.cell.2007.10.036. [PubMed: 18083105]

Stoiljkovic M, Gutierrez KO, Kelley C, Horvath TL & Hajos M (2022). TREM2 deficiency disrupts network oscillations leading to epileptic activity and aggravates Amyloid-beta-Related hippocampal pathophysiology in mice. J. Alzheimers Dis, 88, 837–847. doi:10.3233/JAD-210041. [PubMed: 34120899]

Sudom A, Talreja S, Danao J, Bragg E, Kegel R, Min X, Richardson J, Zhang Z, Sharkov N, Marcora E, et al. (2018). Molecular basis for the loss-of-function effects of the Alzheimer's disease-associated R47H variant of the immune receptor TREM2. J. Biol. Chem, 293, 12634–12646. doi:10.1074/jbc.RA118.002352. [PubMed: 29794134]

Terry RD, Masliah E, Salmon DP, Butters N, Deteresa R, Hill R, Hansen LA & Katzman R (1991). Physical basis of cognitive alterations in Alzheimer's disease: synapse loss is the major correlate of cognitive impairment. Ann. Neurol, 30, 572–580. doi:10.1002/ana.410300410. [PubMed: 1789684]

Terzic B, Cui Y, Edmondson AC, Tang S, Sarmiento N, Zaitseva D, Marsh ED, Coulter DA & Zhou Z (2021). X-linked cellular mosaicism underlies age-dependent occurrence of seizure-like events in mouse models of CDKL5 deficiency disorder. Neurobiol. Dis, 148, 105176. doi:10.1016/j.nbd.2020.105176. [PubMed: 33197557]

Tse K, Puttachary S, Beamer E, Sills GJ & Thippeswamy T (2014). Advantages of repeated low dose against single high dose of kainate in C57BL/6J mouse model of status epilepticus: behavioral and electroencephalographic studies. PLoS One, 9, 1–12. doi:10.1371/journal.pone.0096622.

Ulland TK & Colonna M (2018). TREM2 - a key player in microglial biology and Alzheimer disease. Nat. Rev. Neurol, 14, 667–675. doi:10.1038/s41582-018-0072-1. [PubMed: 30266932]

Ulrich JD, Finn MB, Wang Y, Shen A, Mahan TE, Jiang H, Stewart FR, Piccio L, Colonna M & Holtzman DM (2014). Altered microglial response to Abeta plaques in APPPS1-21 mice heterozygous for TREM2. Mol. Neurodegener, 9, 1–9. doi:10.1186/1750-1326-9-20. [PubMed: 24386896]

Ulrich JD, Ulland TK, Colonna M & Holtzman DM (2017). Elucidating the role of TREM2 in Alzheimer's disease. Neuron, 94, 237–248. doi:10.1016/j.neuron.2017.02.042. [PubMed: 28426958]

Umpierre AD, Bennett IV, Nebeker LD, Newell TG, Tian BB, Thomson KE, White HS, White JA & Wilcox KS (2016). Repeated low-dose kainate administration in C57BL/6J mice produces

temporal lobe epilepsy pathology but infrequent spontaneous seizures. Exp. Neurol, 279, 116–126. doi:10.1016/j.expneurol.2016.02.014. [PubMed: 26896834]

Van Erum J, Van Dam D & De Deyn PP (2019). PTZ-induced seizures in mice require a revised Racine scale. Epilepsy Behav, 95, 51–55. doi:10.1016/j.yebeh.2019.02.029. [PubMed: 31026782]

Verstraelen P, Garcia-Diaz Barriga G, Verschuuren M, Asselbergh B, Nuydens R, Larsen PH, Timmermans JP & De Vos WH (2020). Systematic quantification of synapses in primary neuronal culture. iScience, 23, 1–14. doi:10.1016/j.isci.2020.101542.

Voglein J, Noachtar S, Mcdade E, Quaid KA, Salloway S, Ghetti B, Noble J, Berman S, Chhatwal J, Mori H, et al. (2019). Seizures as an early symptom of autosomal dominant Alzheimer's disease. Neurobiol. Aging, 76, 18–23. doi:10.1016/j.neurobiolaging.2018.11.022. [PubMed: 30616208]

Vossel KA, Ranasinghe KG, Beagle AJ, Mizuiri D, Honma SM, Dowling AF, Darwish SM, Van Berlo V, Barnes DE, Mantle M, et al. (2016). Incidence and impact of subclinical epileptiform activity in Alzheimer's disease. Ann. Neurol, 80, 858–870. doi:10.1002/ana.24794. [PubMed: 27696483]

Wang C, Yue H, Hu Z, Shen Y, Ma J, Li J, Wang XD, Wang L, Sun B, Shi P, et al. (2020). Microglia mediate forgetting via complement-dependent synaptic elimination. Science, 367, 688–694. doi:10.1126/science.aaz2288. [PubMed: 32029629]

Wang Y, Ulland TK, Ulrich JD, Song W, Tzaferis JA, Hole JT, Yuan P, Mahan TE, Shi Y, Gilfillan S, et al. (2016). TREM2-mediated early microglial response limits diffusion and toxicity of amyloid plaques. J. Exp. Med, 213, 667–675. doi:10.1084/jem.20151948. [PubMed: 27091843]

Whitesell JD, Buckley AR, Knox JE, Kuan L, Graddis N, Pelos A, Mukora A, Wakeman W, Bohn P, Ho A, et al. (2019). Whole brain imaging reveals distinct spatial patterns of amyloid beta deposition in three mouse models of Alzheimer's disease. J. Comp. Neurol, 527, 2122–2145. doi:10.1002/cne.24555. [PubMed: 30311654]

Wood JI, Wong E, Joghee R, Balbaa A, Vitanova KS, Stringer KM, Vanshoiack A, Phelan SJ, Launchbury F, Desai S, et al. (2022). Plaque contact and unimpaired Trem2 is required for the microglial response to amyloid pathology. Cell Rep, 41, 1–13. doi:10.1016/j.celrep.2022.111686.

Xia D, Lianoglou S, Sandmann T, Calvert M, Suh JH, Thomsen E, Dugas J, Pizzo ME, Devos SL, Earr TK, et al. (2022). Novel App knock-in mouse model shows key features of amyloid pathology and reveals profound metabolic dysregulation of microglia. Mol. Neurodegener, 17, 1–29. doi:10.1186/s13024-022-00547-7. [PubMed: 34991663]

Yeh FL, Wang Y, Tom I, Gonzalez LC & Sheng M (2016). TREM2 binds to apolipoproteins, including APOE and CLU/APOJ, and thereby facilitates uptake of Amyloid-Beta by microglia. Neuron, 91, 328–340. doi:10.1016/j.neuron.2016.06.015. [PubMed: 27477018]

Yuan P, Condello C, Keene CD, Wang Y, Bird TD, Paul SM, Luo W, Colonna M, Baddeley D & Grutzendler J (2016). TREM2 haplodeficiency in mice and humans impairs the microglia barrier function leading to decreased amyloid compaction and severe axonal dystrophy. Neuron, 90, 724–739. doi:10.1016/j.neuron.2016.05.003. [PubMed: 27196974]

Zarea A, Charbonnier C, Rovelet-Lecrux A, Nicolas G, Rousseau S, Borden A, Pariente J, Le Ber I, Pasquier F, Formaglio M, et al. (2016). Seizures in dominantly inherited Alzheimer disease. Neurology, 87, 912–919. doi:10.1212/WNL.0000000000003048. [PubMed: 27466472]

Zheng H, Jia L, Liu CC, Rong Z, Zhong L, Yang L, Chen XF, Fryer JD, Wang X, Zhang YW, et al. (2017). TREM2 promotes microglial survival by activating Wnt/beta-Catenin pathway. J. Neurosci, 37, 1772–1784. doi:10.1523/JNEUROSCI.2459-16.2017. [PubMed: 28077724]

Zhou Y, Song WM, Andhey PS, Swain A, Levy T, Miller KR, Poliani PL, Cominelli M, Grover S, Gilfillan S, et al. (2020). Human and mouse single-nucleus transcriptomics reveal TREM2-dependent and TREM2-independent cellular responses in Alzheimer's disease. Nat. Med, 26, 131–142. doi:10.1038/s41591-019-0695-9. [PubMed: 31932797]
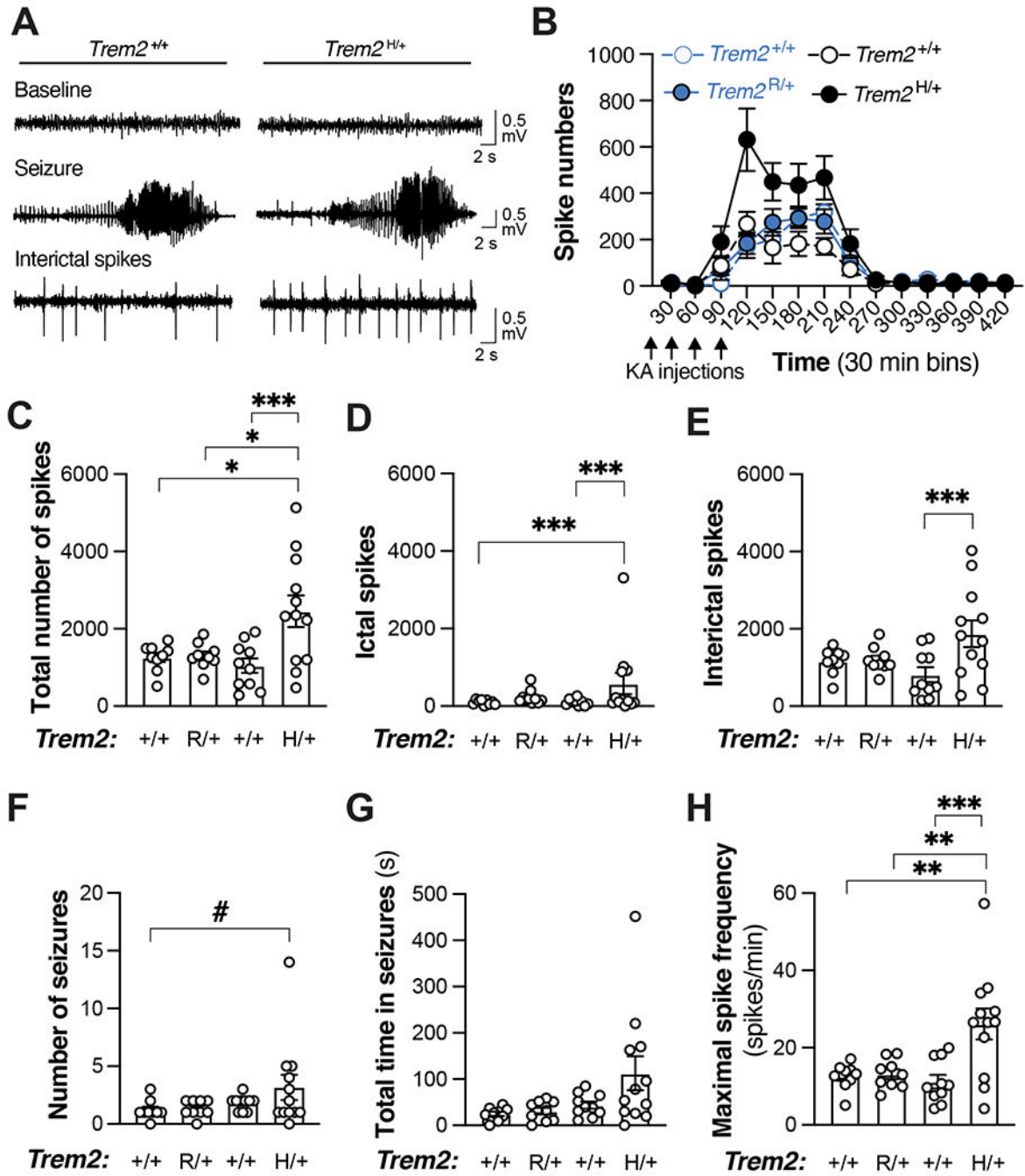
Figure 1. Increased epileptiform activity after excitotoxin challenge in *TREM2*[H/+] mice.
(A to H) Video-EEG recordings were obtained from 5–6-month-old female mice before and after four low-dose KA injections. Knockin mice were compared with WT controls from the respective line as indicated.

(A) Representative EEG traces before (baseline) and after (seizures and interictal spikes) KA injections from a 5-month-old *TREM2*[H/+] mouse and an age-matched WT control.

(B) Spike numbers per 30-min bins recorded during 7 h after the first KA injection, independent of whether spikes occurred during or between seizures.

(C) Total number of spikes during 7 h after first KA injection.

(D) Number of ictal spikes during 7 h after first KA injection.

(E) Number of interictal spikes during 7 h after first KA injection.

(F) Number of seizures during 7 h after first KA injection; no seizure lasted >5 min.

(G) Cumulative amount of time for which mice had seizures during 7 h after first KA injection.

(H) Maximal spike frequency reached within any 30-min bin during 7 h after first KA injection.

n = 9–12 mice per genotype. Data were analyzed by Welch's one-way ANOVA (B), Kruskal-Wallis test (G), or generalized linear model (C to F, and H). These analyses revealed significant group differences in (B to E, and H; $P < 0.01$) but not (G). The number of seizures (F) showed a trend-level difference between $TREM2^{H/+}$ mice and WT mice from the $TREM2^{R/+}$ line. Pairwise comparisons of areas under the curve (AUC) in (B) revealed a significant difference between $TREM2^{H/+}$ mice and WT controls from the $TREM2^{H/+}$ line ($P < 0.05$) and a strong trend toward a difference between $TREM2^{H/+}$ and $TREM2^{R/+}$ mice ($P = 0.06$). $^{\#}P = 0.09$, $*P < 0.05$, $**P < 0.01$, $***P < 0.001$ by Mann-Whitney test followed by Holm-Sidak correction (G) or pairwise comparisons of estimated marginal means followed by Holm-Sidak correction (C to F, and H). In this and the other figures, only statistically significant differences were indicated by brackets and asterisks. Dots in (C to H) represent individual mice. Dots with error bars in (B) and bars in (C to H) are means ± s.e.m.
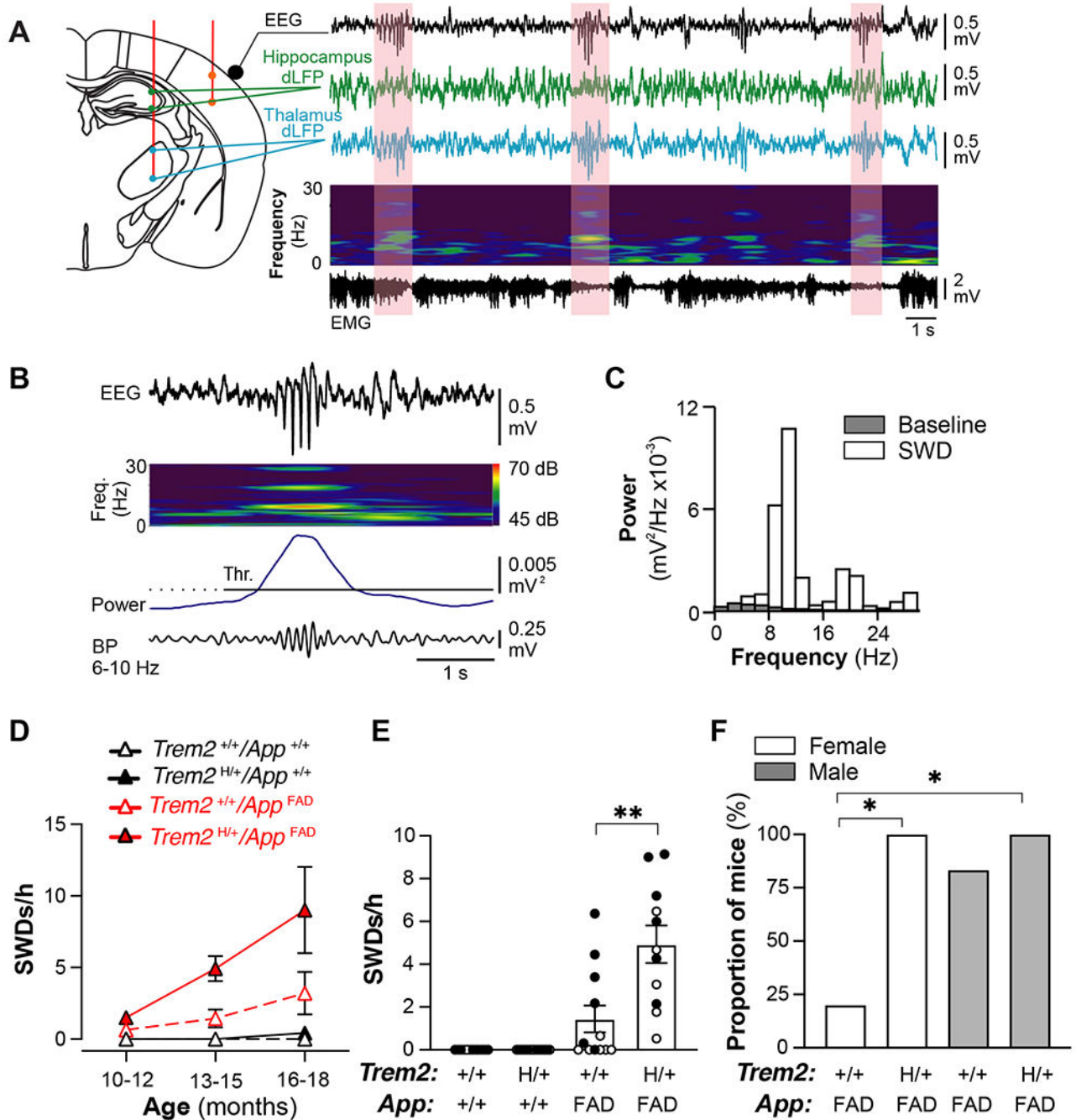
Figure 2. *TREM2*[H] increases the frequency of thalamocortical SWDs in *App*[FAD] mice.
(A to F) Electrophysiological recordings were obtained from freely behaving female and male mice at 10–12, 13–15, and 16–18 months of age.

(A to C) Representative results from a single female *TREM2*[H/+]/*App*[FAD] mouse.

(A) Electrode locations (left) and corresponding traces (right). The EEG was recorded from the primary somatosensory (S1) cortex, the differential local field potentials (dLFPs) from the hippocampus and thalamus, and the EMG from neck muscles. The spectrogram shown above the EMG trace was generated from the EEG recording. Note that the SWDs (pink

shadings) in the cortex and thalamus were associated with changes in the spectrogram (see panel (C) for details) and with reduced EMG activity (indicating behavioral arrest).

(B) Illustration of SWD detection. EEG signals were band-pass (BP) filtered at 6–10 Hz and an SWD detection threshold (Thr.) was applied as described in Methods. dB, decibels. Freq., frequency.

(C) Power spectra calculated from SWDs (white) and baseline (grey) EEG activity. Note the dominant peak frequencies (8–9 and 16–18 Hz) during SWDs.

(D) SWD frequencies detected in female and male mice of the indicated genotypes and ages.

(E) Quantification of SWD frequency in female (empty dots) and male (black dots) mice at 13–15 months of age. No SWDs were detected in WT and $TREM2^{H/+}$ mice at this age. $n =$ 5–8 mice per genotype and sex.

(F) Percentage of female (empty bars) and male (grey bars) $Trem2^{+/+}/App^{FAD}$ and $TREM2^{H/+}/App^{FAD}$ mice with SWDs from (D).

$n = 11$–16 mice per genotype. For (D), we calculated the area under the curve (AUC) and analyzed the data by Kruskal-Wallis test and post hoc Mann-Whitney tests. All pairwise comparisons revealed significant ($P < 0.05$) differences except for $Trem2^{+/+}/App^{+/+}$ vs. $TREM2^{H/+}/App^{+/+}$ ($P = 0.13$). For (E), we used a generalized linear mixed-effects model that treated age, $Trem2$ genotype, App genotype, and the interaction among them as fixed effects and individual mice as a random effect. **$P < 0.01$ based on a pairwise comparison of estimated marginal means followed by Holm-Sidak correction. For (F), Fisher's exact test revealed a significant difference among groups ($P < 0.01$). *$P < 0.05$ by pairwise Fisher's exact test followed by Holm-Sidak correction. Dots in (E) represent individual mice. Dots with error bars (D) and bars in (E) are means ± s.e.m. Bars in (F) represent percentage.

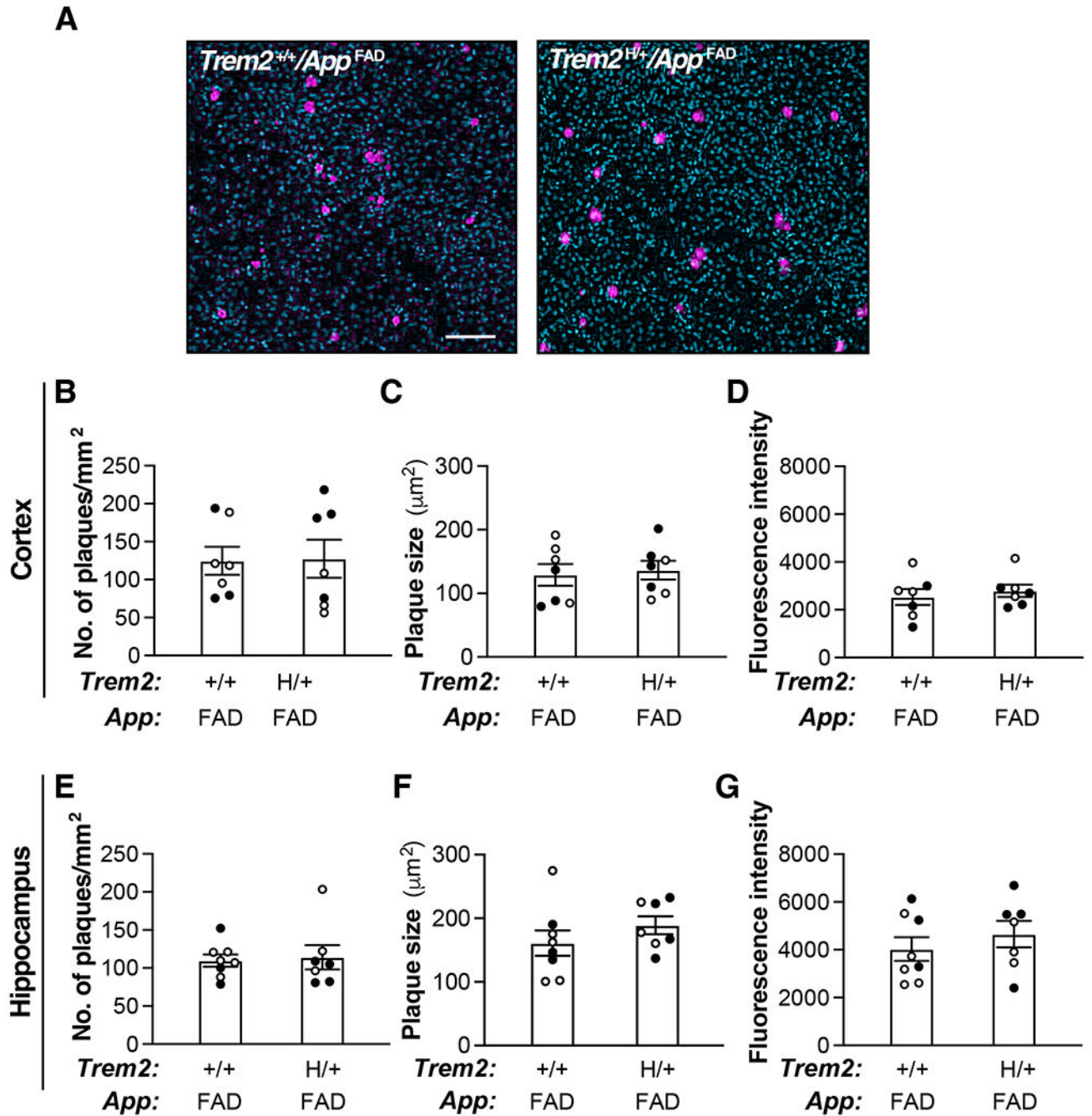**Figure 3. TREM2[H] does not alter plaque levels in the cortex or hippocampus of App^{FAD} mice.**
(A to G) Coronal brain sections from 21–22-month-old female and male mice of the indicated genotypes were stained with ThioS (magenta) and DAPI (cyan) and the parietal cortex was imaged by wide-field microscopy.

(A) Representative images of ThioS-positive plaques in the cortex of female *TREM2^{+/+}/ App[FAD]* (left) and *TREM2[H/+]/App[FAD]* (right) mice. Scale bar: 50 μm.

(B) Number (No.) of plaques per mm² of cortical area.

(C) Plaque size (area covered per plaque) in cortex.

(D) Fluorescence intensity of plaques in cortex.

(E) Number of plaques per mm^2 of hippocampal area.

(F) Plaque size (area covered per plaque) in hippocampus.

(G) Fluorescence intensity of plaques in hippocampus.

n = 7–8 mice per group. Data were analyzed with Student's t-tests. No significant genotype effects were identified. In (B to G), dots represent individual female (empty) and male (black) mice, and bars are means ± s.e.m.
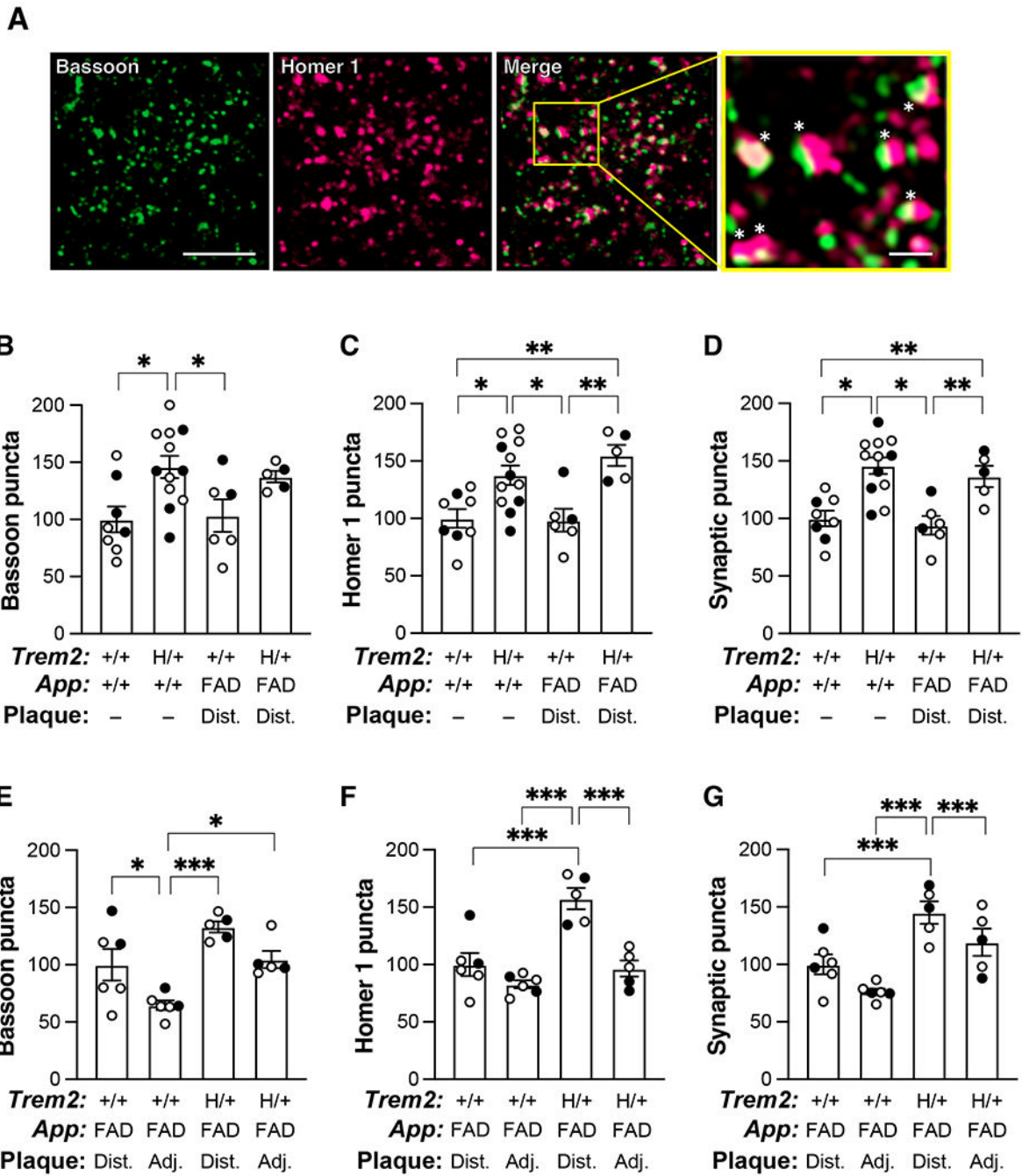
Figure 4. TREM2^H increases cortical synapse density.
(A to G) Coronal brain sections from 21–22-month-old female and male mice of the indicated genotypes were immunolabeled for the presynaptic marker bassoon (green) and the postsynaptic marker homer 1 (magenta), and stained for amyloid plaques with ThioS. The parietal cortex was imaged by confocal microscopy. Synaptic puncta were operationally defined as pairs of bassoon puncta and homer 1 puncta that were <0.5 μm apart. In $Trem2^{+/+}/App^{FAD}$ and $TREM2^{H/+}/App^{FAD}$ mice, we compared cortical regions that were

distal (>20 μm away from plaque perimeter) or adjacent (<10 μm from plaque perimeter) to plaques.

(A) Representative images from the cortex of a female WT mouse illustrate our approach to identifying bassoon-positive presynaptic puncta (green), homer 1-positive postsynaptic puncta (magenta), and synaptic puncta (merge and inset). Scale bars: 5 μm, 1 μm (inset). White asterisks in inset indicate synaptic puncta.

(B to D) Relative densities of bassoon puncta (B), homer 1 puncta (C), and synaptic puncta (D) in plaque-free regions of the cortex in female (empty dots) and male (black dots) mice. For each measure, the mean density in WT mice was defined as 100%.

(E to G) Relative densities of bassoon puncta (E), homer 1 puncta (F), and synaptic puncta (G) in cortical regions that were distal (Dist., data from (B to D)) or adjacent (Adj.) to plaques in female (empty dots) and male (black dots) mice. For each measure, the mean density distal to plaques in $Trem2^{+/+}/App^{FAD}$ mice was defined as 100%.

$n = 5$–12 mice per group. For (B to D), two-way ANOVA revealed a significant effect of the $Trem2$ genotype ($P < 0.001$) but not the App genotype ($P > 0.45$) and no interaction between them ($P > 0.34$). For (e–g), two-way ANOVA revealed significant effects of the $Trem2$ genotype ($P < 0.01$) and plaque adjacency ($P < 0.01$) and a significant interaction between them for (F and G; $P < 0.05$) but not (E; $P = 0.69$). *$P < 0.05$, **$P < 0.01$, ***$P < 0.001$ by Holm-Sidak test. In (B to G), dots represent individual female (empty) and male (black) mice. Bars are means ± s.e.m.
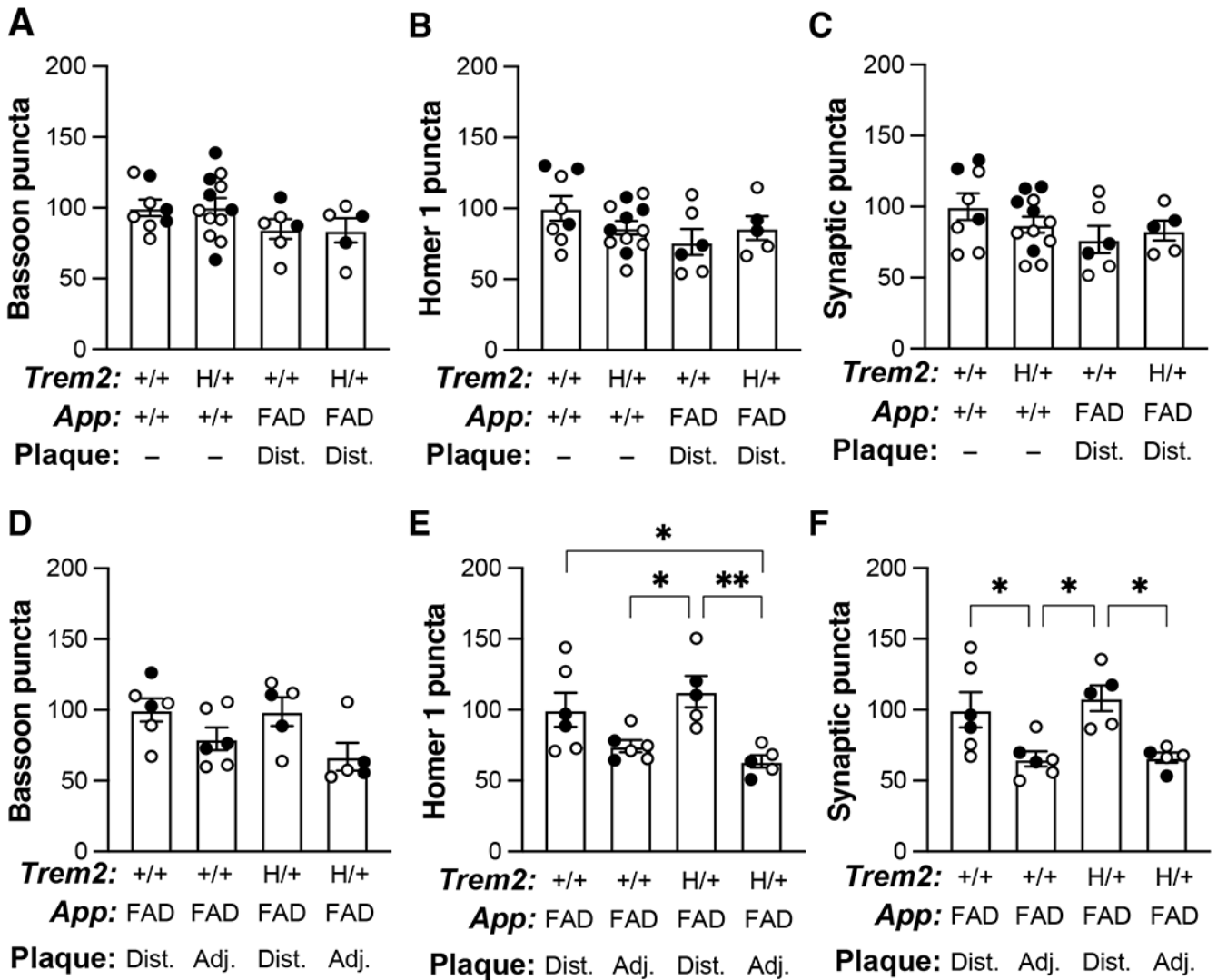
Figure 5. TREM2^H does not alter hippocampal synapse density.
(A to F) Coronal brain sections from 21–22-month-old female and male mice of the indicated genotypes were immunolabeled for bassoon and homer 1, and stained for amyloid plaques with ThioS. The hippocampus was imaged by confocal microscopy. Conventions were otherwise as in Fig. 4.

(A to C) Relative densities of bassoon puncta (A), homer 1 puncta (B), and synaptic puncta (C) in plaque-free areas of the hippocampal CA1 region in female (empty dots) and male (black dots) mice. For each measure, the mean density in WT mice was defined as 100%.

(D to F) Relative densities of bassoon puncta (D), homer 1 puncta (E), and synaptic puncta (F) in CA1 areas that were distal (Dist., data from (A to C)) or adjacent (Adj.) to plaques in female (empty dots) and male (black dots) mice. For each measure, the mean density distal to plaques in Trem2$^{+/+}$/App^{FAD} mice was defined as 100%.

n = 5–12 mice per group. For (A to C), two-way ANOVA revealed no significant effects of the Trem2 (P > 0.46) or App (A: P = 0.0852; B, C: P > 0.13) genotypes and no interaction between them (P > 0.13). For (D to F), two-way ANOVA revealed no effect of the Trem2

genotype ($P > 0.45$) but a significant effect of plaque adjacency (D to F; $P < 0.01$). *$P < 0.05$, **$P < 0.01$ by Tukey test. In (A to F), dots represent individual female (empty) and male (black) mice. Bars are means ± s.e.m.